Distributed deformation and block rotation in 3D

Oona Scotti, Amos Nur, Raul Estevez*

Rock Physics Laboratory
Department of Geophysics
Stanford University
Stanford California 94305
March 1, 1990

ABSTRACT

In this paper, we address how block rotation and complex distributed deformation in the Earth's shallow crust may be explained within a stationary regional stress field. Distributed deformation is characterized by domains of sub-parallel fault-bounded blocks. In response to the contemporaneous activity of neighboring domains some domains rotate, as suggested by both structural and paleomagnetic evidence.

Rotations within domains are achieved through the contemporaneous slip and rotation of the faults and of the blocks they bound. Thus, in regions of distributed deformation, faults must remain active in spite of their poor orientation in the stress field. Traditional friction models cannot account for this mechanism. To solve this problem we developed a model that tracks the orientation of blocks and their bounding faults during rotation in a 3D stress field. Mechanically, we considered Coulomb criteria for rock fracture, as an upper bound, and fault slippage, as a lower bound, between which block rotation is expected.

In our model, the effective stress magnitudes of the principal stresses (σ_1, σ_2, σ_3) are controlled by the orientation of fault sets in each domain. Therefore, (1) adjacent fault sets with differing orientations may be active and may display differing faulting styles, and (2) a given set of faults may change its style of motion as it rotates within a stationary stress regime. The style of faulting predicted by our model depends on a dimensionless parameter $\phi = (\sigma_2 - \sigma_3)/(\sigma_1 - \sigma_3)$. Thus, we present a model for complex distributed deformation and complex offset history requiring neither geographical nor temporal changes in the stress regime.

We apply the model to the Western Transverse Range domain of Southern California. There, it is mechanically feasible for blocks and faults to have experienced up to 75^0 of clockwise rotation in a $\phi = 0.1$ strike-slip stress regime. The results of our model suggest that this domain may first have accommodated deformation along preexisting NNE-SSW faults, reactivated as normal

*now at Universidad de los Andes, Mérida, Venezuela

faults. After rotation, these same faults became strike-slip in nature. Subsequent rotations could have resulted in the present day E-W high angle reverse faults. This history agrees with both prominent structural phases documented for post-Oligocene activity and paleomagnetically inferred rotations of this domain.

CRUSTAL DEFORMATION BY BLOCK ROTATION

1. The problem

Distributed crustal deformation is characterized by sub-parallel sets of faults (Freund, 1970; Freund, 1971; Garfunkel, 1974; Luyendyk et al., 1980; Ron et al., 1984; and others). Sets are distinguished from their neighbors by orientation and often by faulting style as well. In a region like Southern California, throughgoing faults often mark the boundaries of these domains such as the San Andreas and Garlock fault shown in Fig. 1.

If the regional stress field is homogeneous and stationary throughout a region like Southern California (Zoback et al., 1987), then how can we have active fault sets in such varying orientations? At least three solutions can be suggested:
(1) In regions of distributed deformation, fault sets behave in accordance with unknown friction criteria.
(2) The stress field is not homogeneous and stationary. Instead, it changes orientation from one domain to the next.
(3) The stress field is homogeneous and stationary and the fault sets slip in accordance with friction criteria but in some domains blocks and faults rotate.

The answer most probably lies in a combination of these three extreme cases. Fault behaviour is most likely a function of the slip rate and the history of slip; the stress field must be inhomogeneous to some extent across a region of distributed deformation; rotation of blocks and faults must indeed occur when many domains of fault sets coexist.

In this paper, we restrict our attention to the third case: the rotation of faults and of the blocks between them. Accumulating paleomagnetic and structural evidence shows that in region of distributed deformation, many structural domains have rotated in the past, and some are rotating today (see Nur et al., 1986; Ron et al., 1988). Different block rotation mechanisms have been proposed (see Molnar, 1988). Here, we propose a 3D block rotation mechanism based on Nur et al. (1986) 2D model. For this reason, we first give a brief summary of the kinematics and mechanics of the 2D version.

2. Kinematics of block rotation in 2D

The kinematics of block rotation in strike-slip tectonic regimes, were originally proposed by Freund (1970; 1974) on the basis of structural data alone. He observed two sets of strike slip faults with an angle of 145^0 between them measured in the maximun compressional direction. He attributed this angular spread to the tendency of strike slip faults to rotate about a vertical axis away from the maximum compressional direction. In fact, rotation of faults as a mechanism for accommodating deformation, was first recognized in normal tectonic regimes (Ransome et al., 1910; see references in Jackson and White, 1989).

This rotation is illustrated schematically in Fig. 2. In this simple case, the vertical stress $S_v = \sigma_1 = gravity$, is the only stress acting. As the books slide on the shelf they rotate away from σ_1, the direction of maximum compression: in a counter-clockwise (CCW) sense (domain A) or clockwise (CW) sense (domain B) depending on the orientation of the books. From this example, one can see that—whether strike-slip or dip-slip— right-lateral fault motion leads to CCW sense of rotation, and left-lateral movement leads to CW sense of rotation of blocks and faults.

The block rotation model assumes that the rotating blocks are rigid. Luyendyk et al. (1985), Ron et al. (1984), Carter et al. (1987) and Terres and Luyendyk (1985) have validated this assumption. In the domains they studied, two significant correlations were found. The first one between the measured sense of

slip, the expected sense of rotation and the paleomagnetically inferred axis of rotation (as explained in Fig. 2); the second one between the known amount of total displacement across a fault set, the measured average spacing between sub-parallel faults, and the amount of rotation inferred paleomagnetically for a domain.

3. Mechanics of block rotation in 2D

In Freund's model, as faults slip, the blocks they bound rotate away from the direction of maximum compression. Nur et al. (1986) added a mechanical limit to this kinematic model for the case of vertical strike slip faults rotating in a strike-slip regime. In Nur's block rotation (BR) model, two additional constraints are introduced. One is given by the Coulomb criterion for sliding, and the second one by the Coulomb criterion for fracturing (eq. (1) and (2) in the Appendix).

Within a region of distributed deformation, where a single fault set orientation characterizes each domain, the first constraint implies that fault sets may remain active even if poorly oriented in the stress field, and the second constraint sets a limit on how poorly oriented the fault set may become. A fault is considered optimally oriented when the intermediate stress σ_2 is contained in the plane of the fault and the shear stress required for slip along the fault is such that the $\sigma_1 - \sigma_3$ Mohr circle is just tangent to the sliding line (Fig. 3).

In Nur's model, faults rotate within a stationary stress field. This implies that during rotation the stress magnitudes must change in a domain, for blocks and faults to continue to slip and rotate (Fig. 4). When the magnitude of the differential stress reaches the strength of the intact crust (the fracture line on the $\sigma_n - \tau$ plot), a new set of more optimally oriented faults forms, and the old set becomes locked. As a result, a discrete range of fault orientations is predicted by the BR model. Only when sufficiently large rotations occur in a domain will cross-cutting generations of fault sets give rise to a complex pattern of faulting, such as those observed in situ (Angelier et al., 1985; Ron et al, in press).

The mechanical constraints of the BR model provide an important step toward quantitative estimates of the contribution of block rotation to distributed deformation in the Earth's crust. The relationship among friction, strength and the amount of rotation that a single set of faults can experience are detailed in Nur et al. (1986).

As Fig. 4 shows, block rotation can cause poor fault orientation. However, the 2D model is limited in its application since the intermediate principal stress σ_2 must remain in the fault plane. This limitation prevents any change of faulting style during rotation. A 3D formulation is necessary to model the more common case of rotation along reactivated faults, where σ_2 is not necessarily in the plane of the fault. Then, we can identify the conditions that allow a fault set to drastically change its behaviour as it rotates.

4. Block rotation in 3D

The focus of this paper is to understand distributed deformation and the relationship between fault slip and the rotation of faults and blocks in a three dimensional stress field. The fundamental strenght and friction criteria proposed in the 2D model are preserved. In addition, the 3D model considers all faulting styles that can occur in a general stress field for any starting orientation of modeled faults.

We will first discuss the more fundamental assumptions that must be made when modeling distributed deformation and block rotation in a 3D stress field. Then, we will discuss the implications of combining the 3D stress Mohr circle

with friction criteria applied to the present-day tectonics of Southern California. In the main part of the paper, we will discuss the principles of the 3D BR model. As the results will show, even a simple 3D BR model can produce complicated faulting histories and complex distributed deformation geometries.

Because faults generally change their behaviour as they rotate in a stationary stress field, a model of faulting and rotation in 3D is fundamental to our understanding of this mechanism. In the final part of the paper, as a practical application of our model, we will compare the known rotation history of the Western Transverse Range domain in Southern California with the results of our model. We find encouraging similarities between our 3D BR model predictions and the complex structural and geological record of this domain.

THE STATE OF STRESS

1. One principal stress assumed vertical

Following Anderson (1951), the vertical stress S_v is assumed to be a principal stress. The magnitude of S_v determines the tectonic stress regime: normal if $S_v = \sigma_1$, reverse if $S_v = \sigma_3$, and strike-slip if $S_v = \sigma_2$ —where $\sigma_1 > \sigma_2 > \sigma_3$ and compressive stresses are positive. Note that beyond Anderson's view, a given tectonic stress regime does not imply a specific faulting style. Particularly in regions of distributed deformation because they are characterized by domains of fault sets.

2. Stress models

As shown in Fig. 4 for the 2D case, stress magnitudes must change in a domain because we assume that faults and blocks rotate within a stationary stress field. Since we do not know how this change may take place, we must make a number of simplifying assumptions. One possible assumption is that the volume of the crust being deformed remains constant so that hydrostatic stress is constant

$$\sigma_1 + \sigma_2 + \sigma_3 = constant$$

Another possibility is that the stress ratio ϕ remains unchanged

$$\phi = \frac{\sigma_2 - \sigma_3}{\sigma_1 - \sigma_3} = constant$$

The stress ratio $\phi = (\sigma_2 - \sigma_3)/(\sigma_1 - \sigma_3)$ is often used as a dimensionless parameter to describe the 3D state of stress in the Earth's crust. It may vary from $\phi = 0$ when $\sigma_2 = \sigma_3$ to $\phi = 1$ when $\sigma_2 = \sigma_1$.

3. Fault geometry representation in 3D

Whatever assumptions are made, we need a way of tracking fault plane orientations during rotation in a 3D space. In this paper, we use two representations: the Mohr circle, which plots the orientation of faults in a $\sigma_n - \tau$ plane, and the Wulff-projection stereonet, that plots the orientation of fault planes in the principal stress axis reference.

THE 3D MOHR CIRCLE

In 2D space, a single angle defines fault orientation. In 3D space, two angles are required to define a pole to a fault plane. Fig. 5a shows how these angles are

represented in the Mohr circle. For a more complete treatment of the 3D Mohr circle representation we refer the reader to Jaeger and Cook (Chp 2.6, 1969). Let us consider here only three extreme cases:
(1) pole P_2 which falls exactly on the $\sigma_1 - \sigma_3$ circle: this is equivalent to the 2D representation in which σ_2 is in the plane of the fault.
(2) pole P_1 which falls exactly on the $\sigma_3 - \sigma_2$ circle: in this case σ_1 is in the plane of the fault and
(3) pole P_3 which falls exactly on the $\sigma_2 - \sigma_1$ circle: in this case σ_3 is in the plane of the fault.
When a pole (P) falls in the shaded region in Fig. 5a, then all three principal stresses are off the plane of the fault. In this case α_1 and α_3, the angles that the fault plane normal makes with σ_1 and σ_3 respectively, are calculated by drawing two circles concentric with the two small $\sigma_1 - \sigma_2$ and $\sigma_2 - \sigma_3$ circles and passing through the pole. Then the intersection of the $\sigma_1 - \sigma_2$ concentric expansion with the $\sigma_2 - \sigma_3$ circle defines α_3, and the intersection of the $\sigma_2 - \sigma_3$ concentric expansion with the $\sigma_1 - \sigma_2$ circle defines α_1 as shown in Fig. 5a. The Mohr circle representation is powerful because it represents stress magnitudes, friction criteria and the geometry of faults in the stress field, all in one graph.

THE WULFF-PROJECTION

The same fault normals shown in Fig. 5a are plotted on a Wulff lower hemisphere projection in Fig. 5b: P_2 plots on the line joining the $\sigma_1 - \sigma_3$ directions, P_1 plots on the line joining the $\sigma_2 - \sigma_3$ directions and P_3 plots on the line joining the $\sigma_1 - \sigma_2$ directions. Depending on the stress regime, either σ_1, σ_2 or σ_3 is represented in the down orientation throughout the paper. This type of representation is often used by structural geologists because it makes it easier to visualize the geometry of faults in the stress field.

4. Choice of material parameters

Finally, we need to assume some values for the mechanical constraints of the BR model. The relationship between material parameters and block rotation is discussed in detail in Nur et al. (1986). As we will see for the case of the Western Transverse Range, the specific values do not affect the qualitative aspect of the results. In this paper, we are more concerned with the changing behaviour of faults as they rotate. In the model, we assume the following values for the material parameters (Handin, 1969): 1.0 for the coefficient of friction of intact rock (it could be much greater) and 0.6 for the coefficient of friction of preexisting faults (it could be less). 1000 bars for the cohesion of intact rock (could be greater) and 50 bars for the cohesion of preexisting faults (could be 0). Given these values, the stress limits (Coulomb criteria) employed in the model become:
(1) The upper limit, representing the strength of the crust (the fracture line)

$$\tau_0 = 1000 + 1.0\sigma_n \quad (in\ bars)$$

(2) The lower limit, representing the strength of preexisting faults (the sliding line)

$$\tau_f = 50 + 0.6\sigma_n \quad (in\ bars)$$

(3) the tensile limit, assuming the crust cannot withstand any tensile stress

$$\sigma_3 \geq 0 \qquad (\sigma_3 < \sigma_2 < \sigma_1)$$

3D MOHR CIRCLE: A KEY TO MIXED STYLES OF FAULTING

In a three dimensional situation, the value of the intermediate stress plays a key role in determining the style of faulting. This contrast with the two dimensional one where σ_2 is always in the fault plane. By itself, this result is not new (Bott, 1959; McKenzie, 1969; and others). However, here we include σ_2 specifically to allow us to understand how active faults become poorly oriented during 3D block rotation. Before considering block and fault rotation, let us first enlist the help of the Mohr circle to see when preexisting faults can be reactivated—and what this means for regionally distributed deformation in Southern California.

1. Friction criteria and the 3D Mohr circle

Clearly, reactivation of preexisting faults is constrained by the strength of the crust, the strength of the faults and the relative magnitudes of the three principal stresses. Jaeger and Rosengren (1969) discuss the influence of these parameters in more detail. Let us consider the material parameters values discussed in the previous section and a σ_3/σ_1 ratio exceeding the sliding line but not the fracture line, as shown in Fig 6.

Consider only three sets of preexisting faults as sketched in Fig. 6: (a) set 1 which contains the σ_1 direction, (b) set 2 which contains the σ_2 direction and (c) set 3 which contains the σ_3 direction. The faulting styles expected along each fault set are also sketched. They depend on the tectonic stress regime and the orientation of each fault set. The normals to actively slipping faults plot within the shaded region of the Mohr circle. The size of the shaded region depends on the σ_3/σ_1 ratio and the ϕ value. Assuming low σ_3/σ_1 ratio, at lower ϕ values, say less than 0.4, all three fault sets will be active. In the normal regime, set 1 will be reactivated as strike-slip faults, set 2 and set 3 as normal faults. In the reverse regime set 1 and set 2 will be reactivated as reverse faults and set 3 as strike-slip faults. In the strike-slip regime, set 1 will be reactivated as normal faults, set 2 as strike-slip faults and set 3 as reverse faults. At ϕ values exceeding 0.4, fault set 3, which contains σ_3 in its plane, will be locked, while the other two fault sets can be reactivated.

These cases represent the most extreme styles of faulting that can be expected in the three tectonic stress regimes. Clearly in a domain characterized by an obliquely slipping fault set, movement could occur if it plotted within the shaded region of the 3D Mohr circle. A summary table for the limiting cases is provided in Table 1.

Stress Ratio	Tectonic stress regime			Faults
	normal $S_v = \sigma_1$	*reverse* $S_v = \sigma_3$	*strike-slip* $S_v = \sigma_2$	
low	normal	reverse	strike-slip	set 2
$0. < \phi < 0.4$	strike-slip	reverse	normal	set 1
	normal	strike-slip	reverse	set 3
high	normal	reverse	strike-slip	set 2
$0.4 < \phi < 1.0$	strike-slip	reverse	normal	set 1

Table 1. *Limiting cases of faulting styles expected in three tectonic stress regimes as functions of the stress ratio* $\phi = (\sigma_2 - \sigma_3)/(\sigma_1 - \sigma_3)$*—for each of the three*

sets aligned with one of the principal stresses in their planes and for a low σ_3/σ_1 ratio.

2. Southern California domains: an example of distributed deformation

Southern California is characterized by domains of faults separated by throughgoing boundary faults (Fig. 1). The shaded regions in Fig. 1 represent domains where block rotation has been inferred (Luyendyk et al., 1985) and therefore where we expect faults to be poorly oriented in the present-day stress field. Whatever the stress field orientation, we do observe a mixture of faulting styles. In the Western Transverse Range domain (WTR), high-angle reverse-oblique slip along E-W trending faults has been documented (Lee et al., 1979; Yerkes and Lee, 1979a,b). In the Mojave domain (MOJ), Sauber et al. (1986) have described right-lateral strike-slip along NW-SE trending vertical faults. In the East Transverse Range domain (ETR), activity is left-lateral strike-slip along E-W trending vertical faults (Jones, 1988; Powell, 1982).

Can this diverse fault behaviour be the result of a regionally stationary stress field—in accordance with friction criteria? Note first how the San Andreas strike-slip system dominates the region's tectonics. Consider next, from the arguments above and Table 1, that reverse and strike-slip faulting may coexist within a low ϕ strike-slip stress regime and low σ_3/σ_1 ratio. Lastly, we need an estimate of the σ_1 direction and of the value of μ_f, the coefficient of frictional sliding, to apply the 3D BR model to this region. Both, the σ_1 direction and the μ_f value, are constrained by the orientation of strike-slip faults in the MOJ domain and of high angle reverse faults in the WTR domain: σ_1 must trend $N20^0E$ and $\mu_f = 0.4$ for MOJ and WTR faults to slip. Representative fault plane solutions shown in Fig. 1 are plotted on the 3D Mohr circle of Fig. 7. The plot is normalized by the value of σ_1, assuming a depth of faulting of 5–10 kms, an orientation of σ_1 trending $N20^0E$, a $\mu_f = 0.4$ and a $\phi = 0.1$. Faults of the ETR, as well as those of the WTR and MOJ domains, plot closely to the sliding line. Therefore, in our simple model of distributed deformation, faults sets in all three domains can slide in accordance with friction criteria in a regionally stationary strike-slip regime.

The BR model can not presently account for slip along domain bounding faults (Fig. 1). In fact, the model predicts that very little shear stress is resolved on the San Andreas fault, the major throughgoing boundary fault in this region. While this agrees with recent borehole findings at Cajon Pass (Zoback et al., 1987), questions remain concerning the mechanics of lithospheric faults, but they are beyond the scope of this study.

In summary, we see discrete fault orientations that separate into domains. In Southern California, even poorly oriented fault sets can slip in a σ_1 $N20^0E$ directed strike-slip regime with $\phi = 0.1$ and $\mu_f = 0.4$. We will return to these values in the final part of the paper when discussing the faulting history of the WTR domain.

A fundamental question must be considered at this point: how do faults that presumably form in a favorable orientation become poorly oriented? As mentioned previously, extensive paleomagnetic studies (references in Luyendyk et al., 1985 and Dokka, 1989) indicate that these domains have undergone a complex history of deformation characterized by rotations about a vertical axis. In the following section, we hope to demonstrate that block rotation in a 3D stationary stress field provides a simple mechanism to accommodate distributed deformation that explains, in accordance with friction criteria, those rotations

that have been documented.

3D BLOCK ROTATION

In the previous section, we defined conditions in a 3D stress field under which reactivation of poorly oriented faults can occur (Table 1). We showed that domains of poorly oriented faults can be active in a regionally stationary stress field if the limits for the differential stresses in the Earth's crust lie between the upper bound (rock strength) and the lower bound (fault strength).

We will now investigate a process which allows faults, to pass from optimal to poor orientation; this is the rotation of blocks and their associated faults. Block rotation was modeled kinematically in 2D by Freund (1974), Garfunkel (1974) and Ron et al. (1984) and mechanically in 2D by Nur et al (1986). In this paper we present a 3D mechanical modeling program. Given strength and friction values, our model computes both the maximum rotation possible for a given fault set, and the conditions needed to induce a change of faulting style for that set.

1. The model

The block rotation model (BR) describes idealized domains of fault sets in situ. Faults in a set are typically sub-parallel, so it is reasonable to consider the rotation history of one fault to be representative of the entire set. In the BR model, we assume that all faults in a given set are active simultaneously. Thus, deformation remains uniform throughout the domain. We also assume that the rotating blocks are rigid. Faulting is therefore brittle. We expect a a detachment at depth (ca. 15 kms), that decouples upper crustal rotations from lower crustal ductile shear.

In the brittle upper crust, we require four main assumptions for the 3D BR model. The first, a mechanical constraint, assumes that the Coulomb criterion controls sliding of faults in the set. The second assumes that fault slip is directed along the maximum resolved shear stress for the fault. The third, a kinematic constraint, assumes that both blocks and fault planes rotate away from the σ_1 direction. The fourth and final assumption is the stationarity of the principal stress directions. Thus, once fault sets have slipped and blocks rotated, stress magnitudes must change to allow further slip and rotation.

To facilitate the analysis, we assume that the magnitude of the principal vertical stress S_v remains constant throughout rotation. The other two stress magnitudes vary to conserve stress ratio ϕ (see Appendix for discussion). As mentioned earlier, more general stress histories are possible but they require additional information. Here, we present results for a constant ϕ stress history only.

Given a stress model and a stationary direction of the stress field, we must keep track of the fault orientation during rotation. Two new concepts are introduced: the stress path and the rotation path of a rotating fault set. These concepts form the basis of the 3D BR model. Estevez et al. (1987) discussed the stress path concept in considerable detail. The derivation is summarized in the Appendix here. This paper will focus mainly on the rotation path concept. The rotation path of a rotating fault set can be represented on a Mohr circle, as the successive (σ_n, τ) values of the fault set on the Coulomb sliding line, and on the Wulf-projection, as the subsequent positions of the fault set in the stress field.

2. 2D rotation path

The rotation path, a fundamental concept of 3D fault rotation, is illustrated

schematically on a 2D Mohr circle in Fig. 8. Assume that a given domain contains one preexisting fault set with its normal aligned at α_1 from the σ_1 direction (Fig. 8a, point 1). For the fault set to slip, the stress must rise from point 1 to point 2. By the Coulomb criterion, shear stress at point 2 can drive the fault set into motion. At slip, the fault set rotates, eventually assuming an orientation α_2 (Fig. 8b). The angles α_1 and α_2 represent fault normals! Therefore, as blocks and faults rotate away from σ_1, normals to faults approach the σ_1 point along the σ_n axis—as shown earlier in Fig. 4. Thus during rotation fault normals move from point 2 to point 3. In time, with increasing stress, the fault normal will continue to rotate. When point 4 is reached (Fig. 8c), the Coulomb fracture criterion will come into play—the fault will be locked at position α_3, and a new set of faults will be created (point 5 in Fig. 8c). The path followed from point 2 to point 4 is the rotation path for Nur's 2D model.

Unfortunately, a 2D model is limited to analysis of the special case where σ_2 lies within the preexisting fault set. To model faults rotating more generally within the stress field, we must study the 3D case.

3. 3D rotation paths

Many rotation paths are possible in 3D, but we will consider only three limiting cases, shown in Fig. 9. As described earlier, faults slip and rotate in the BR model, as long as the stress limits and the Coulomb sliding criterion are satisfied. By assuming a constant ϕ stress history, we can plot the rotation path of a fault set on Mohr circles normalized by σ_1. Thus, rotation paths plot as curved lines, reflecting the variation, with fault rotation, in the absolute magnitudes of the principal stresses.

For a given stress regime, we would like to determine the style of faulting exhibited at every point along the rotation path of a fault set. This style can be characterized by the rake, or the direction of slip of the fault's hanging wall along the footwall, as shown in Fig. 10. Because the fault plane itself is also rotating, we must track this change as defined by fault plane strike and dip, or more simply by the orientation of the fault normal in 3D space.

In the following section, we present the results of 3D BR modeling. We have assumed stationary stress orientations and constant ϕ during rotation. Separately, we discuss modeled changes in faulting style (rake) and attitude (strike and dip) for the three specific fault sets, as functions of both the stress ratio ϕ and the tectonic stress regime.

3D BLOCK ROTATION: RESULTS

Rotation paths for the three limiting cases (Fig. 9) are summarized in Fig. 11 and Fig. 12. In each figure, results are shown for the three stress regimes, at low, intermediate and high ϕ values. Fig. 11 displays changes in faulting style as a function of rotation in its nine *rotation/rake* plots. The columns represent the three ϕ cases, and the rows represent the three tectonic regimes. The faulting style along the rotation path, that is the rake of a fault set, is determined by the fault set orientation and the ϕ value: the higher the ϕ value the more stable the rake becomes during rotation. This is illustrated by the Mohr circle plots (bottom row in Fig. 11): as the the $\sigma_2 - \sigma_3$ circle grows, the $\sigma_1 - \sigma_2$ circle shrinks, and rotation paths stop farther away from the $\sigma_1 - \sigma_2$ circle.

Fig. 12 displays the fault set attitude for the same rotation paths shown in Fig. 11. The columns still represent the three ϕ cases, but Fig. 12a,b,c represent the normal, reverse and strike-slip regime seperately. 3D motion is shown by plotting rake vs. strike, rake vs. dip and strike vs. dip along the rotation path. Rotation paths are plotted on Wulff-projections at the bottom of Fig. 12, to help

visualize the changing orientation of fault sets during rotation in a stationary, $\phi = constant$ stress field. Notice, again, the stabilizing effect of high ϕ values displayed by the shape of the rotation path. The dominant σ_1 at $\phi = 0.1$, drives all three paths very close to its direction. Some curvature of the paths can be noticed at $\phi = 0.5$, while straight paths characterize the $\phi = 0.9$ case— where σ_1 and σ_2 are nearly equal in magnitude.

Let us consider each rotation path in more detail. The initial orientation of pole 3 in Fig. 11 and 12, for example, closely contains the σ_2 direction in the planes of its fault set. This makes it equivalent to the 2D block rotation case—the intermediate stress σ_2 plays no part in this pole's rotation path. The rake (Fig. 11) remains unchanged during rotation under any value of ϕ: normal regimes produce normal slip. Likewise, reverse and strike-slip regimes yield reverse and strike-slip motion, respectively. Thus, our assumption that one principal stress axis is vertical has precluded oblique slip in the 2D case of pole 3.

Pole 1 and pole 2, however, are influenced by σ_2. As a result, their faulting style changes under rotation—sometimes dramatically. Surprisingly complex patterns of nonlinear rotation paths are outlined for these fault sets in Fig. 11 and 12. Note that these changes take place under fixed ϕ values and stationary principal stress directions.

Changing faulting style—Rake

As mentioned earlier, higher ϕ values have a stabilizing effect. Thus, rakes for the rotation paths of pole 1 and 2 in Fig. 11 are nearly constant during rotation in all three stress regimes. At lower values of ϕ, however, the model yields surprising rake histories for the rotation paths of these poles. In the normal stress regime, strike-slip fault sets may rotate into pure normal fault sets. In the reverse stress regime oblique-slip fault sets with a large component of strike-slip may rotate into a reverse slip fault set (pole 2) or a strike-slip fault set (pole 1).

The strike-slip stress regime displays the most dynamic results of the 3D BR model.The results suggest that it is possible for pure normal fault sets (pole 1) to rotate into a strike-slip one, and subsequently into a reverse-oblique slip fault set—all within a strike-slip regime! Even at intermediate ϕ values, dramatic changes take place in the rakes of pole 1 and 2, although they converge to strike-slip motion upon rotation. High ϕ values limit rake changes during rotation, as always, but pole 2 does tend towards a more strike-slip motion.

The 3D BR model predicts rotations of up to 75^0 (each rotation step corresponds to 5^0 of rotation) for the most poorly oriented fault sets. By considering these limiting cases, we have modeled rotations much greater than those of Nur et al. (1986), and we have also found cases where the faulting style may reverse during the rotation path of a single fault set.

Changing fault orientation—Strike and Dip

Fig. 12 has been designed to express 3D rotation about oblique axes as as a function of dip, strike and rake—to better visualize fault rotation in 3D. Again the stabilizing effect of higher ϕ values is observed in all three stress regimes (Fig. 12a,b,c).

Results of the model for the normal stress regime are detailed in Fig. 12a. Considering the low ϕ column on the left, one can see how all three paths change mostly in dip. This horizontal axis of rotation is what one might typically expect for a normal stress regime, and the 3D BR model concurs. Intermediate ϕ values suggest greater changes in strike during rotation, while at high ϕ values the model predicts— surprisingly so—that strike changes more than dip, particularly

for pole 1. Vertical-axis rotation, usually associated with strike-slip regimes, is therefore possible in normal stress regimes as well.

The results for the reverse stress regime shown in Fig. 12b, predict rake changes throughout rotation at low ϕ values. Poles 1 and 2 are expected to change more in strike than in dip. Again, we see how the 3D BR model predicts vertical-axis rotation of fault sets—this time in a reverse stress regime. Increasing ϕ values induce predominantly steepening of the fault planes during rotation, resulting in the more familiar horizontal-axis rotations.

The results for the strike-slip stress regime shown in Fig. 12c, represent the most striking results of the 3D BR model. Interestingly, the low ϕ case allows for decreasing dip during normal slip, followed by a steepening of the dip when the rake becomes reverse. In the strike-slip regime, the model predicts that most fault sets will follow an oblique axis of rotation. One notable exception, though, can be found in the $\phi = 0.9$ case, where pole 1 rotates unexpectedly about a horizontal axis in a strike-slip regime.

To summarize the results of our model, three specific initial orientations of fault sets were studied in nine different combinations of ϕ values ($\phi = 0.1, 0.5, 0.9$) and stress regimes ($S_v = \sigma_1, \sigma_2, \sigma_3$). In each case the predictions of the model were presented using the rotation path. Along this path we analyzed behaviour (rake) and attitude (strike and dip) of the fault set as it rotated in a stationary, $\phi = constant$ stress field.

The most important conclusions of our results are: first, that for most cases the results predict an oblique axis of rotation, and second that during rotation, as faults change their orientation in the stress field, the style of faulting may change as well—sometimes dramatically.

A direct consequence of these result is that paleomagnetically inferred rotations may not be directly related back to a specific tectonic stress regime. Indeed, rotations about vertical axes, while usually found in strike-slip stress regimes (Hornafius, 1986; Kamerling and Luyendyk, 1985; and others), have been documented in normal stress regimes as well (Li et al., 1990; Pavlides et al., 1988; Hudson and Geissman, 1987; Kissel et al. 1986; Brown and Golombek, 1986; Jackson and McKenzie 1984; 1983). Paleomagnetism is an invaluable aid to decipher complex histories of rotation in regions of distributed deformation. Our 3D BR model provides a framework within which, paleomagnetic, structural and stress data can be combined to better understand complex rotation histories. We analyze such a case in the following section, to demonstrate the application of the 3D BR model to actual complex tectonic problems.

A 3D BLOCK ROTATION EXAMPLE: THE WESTERN TRANSVERSE RANGE

The shear motion between the Pacific and the American plates in Southern California is distributed across a 200 km wide zone which consists of a complex array of block-faulted domains (Fig. 1; Luyendyk et al., 1985). In the first part of the paper, we showed (Fig. 7) how mixed styles of faulting observed today in this region can be explained in a stationary strike-slip stress regime. Now, we apply the results of the 3D BR model to the rotation history of one of these domains, namely the Western Transverse Ranges (WTR).

1. Tectonic history

The WTR domain is a region limited to the north by the Santa Ynez fault, to the south by the Malibu fault system, to the west by the Hosgri fault and to the east by the San Gabriel fault (see WTR in Fig. 1). The right-lateral shear between the Pacific and North American plates since Oligo-Miocene time

should have dominated the tectonic history of this domain. From the geological record alone, however, the tectonic history seems much more complex. This is documented by detailed stratigraphic and structural studies (Yerkes et al.,1981; Luyendyk et al., 1985; Yeats, 1987; Namson and Davis, 1988 and others). The following discussion is concerned with the most prominent deformational phases documented for this region—simplified for the purpose of this study.
Phase I: in late Oligocene to early Miocene time, there was deposition of sediments in elongate normal-fault controlled basins which are presently oriented east-northeast (Terres and Lyuendyk, 1985).
Phase II: a mixture of strike-slip and normal faulting characterized the extentional tectonics of Miocene times (Yeats, 1987).
Phase III: a significant period of compression followed at the beginning of the Quaternary, overprinting all previous events. Structural evidence suggests (Yerkes and Lee, 1979a) that "at the present rates all the measured compressive deformation within the WTR could have occurred during the last 0.5 to 1 m.y.". Namson and Davis (1988) describe this last phase of north-south convergence in detail.

This sequence of phases is shown schematically in Fig. 13: a rake of 90^0, representing the normal faulting period—phase I is followed by a rake of 0^0, representing the strike slip faulting period—phase II, leading to a rake of -65^0, representing the present day period of reverse oblique faulting—phase III.

With the advent of paleomagnetic studies carried out in many domains across Southern California (Luyendyk et al., 1980; Terres and Luyendyk, 1985; Hornafius, 1986: Carter, 1987), it appears that block rotation has been the predominant mechanism of deformation in this region. Paleomagnetic interpretations indicate that since mid-Miocene time, the Transverse Ranges have experienced significant block rotations about a vertical axis—particularly in the WTR domain, where up to 90^0 of rotation is estimated.

According to Luyendyk and his co-workers, the WTR clockwise rotations were associated with left-lateral slip on a set of vertical, strike-slip faults originally N-NE trending. The faults defined blocks about 100-200 kms long and 10 kms wide that rotated as rigid bodies away from the direction of compression.

The structural history for the WTR, as suggested by Terres and Luyendyk (1985), is explained by three separate set of faults formed under three different stress regimes (Fig. 13). A set of N-NE striking normal faults formed during the extensional phase (I), another set of strike slip faults, which rotated with the blocks, formed during the shearing phase (II), and yet another set of E-W striking high-angle reverse faults formed during the present-day compressional phase (III).

While kinematic knowledge has improved our understanding of the WTR structural history, the story it tells is complex. By combining the frictional constraints of the 3D BR model with paleomagnetic, structural and geological data, we can now show how one set of faults, preexisting and rotating in a stationary strike slip stress field, can account for all three deformational phases.

2. The 3D BR model for the WTR

How can we use the results of Fig. 11 and 12 to help us understand the history of rotation of the WTR? Let us start with the simplest assumption: the stress directions remained stationary, in the present day orientation, throughout the post-Oligocene deformation history of the domain. From the first part of the paper, we know that it is possible for the WTR fault set to slip in a oblique reverse motion in a strike-slip regime with σ_1 $N20^0E$ directed, if $\mu_f = 0.4$ and $\phi = 0.1$. Consequently, we can expect the modeled rotation path that best describes the deformation of the WTR domain to be similar to that of pole 1 in

Fig. 11, for the case of the strike slip regime and $\phi = 0.1$, where the final value of the rake is oblique reverse.

The results shown in Fig. 11 and 12 are for $\mu_f = 0.6$. To model the faults of the WTR domain we must re-run the program with $\mu_f = 0.4$. Fig. 14a shows the stress regime and the rotation path modeled for the WTR domain. Fig. 14b shows how lowering the coefficient of frictional sliding allows faults to rotate further away from σ_1. The shape of the rotation path remains the same, but the limits within which a fault set may rotate change. In our case, faults may rotate until a steeper dip is achieved (compare strike and dip for the final orientation of pole 1 in Fig. 12c and Fig. 14b).

But what does this rotation path tell us about previous fault behavior and previous geometries of faulting? Fig. 14b displays the structural history predicted by the model for this rotation path. The rake starts at an initial value near pure normal slip, a time of "extension" similar to phase **I**. Upon fault and block rotation, the rake becomes pure strike-slip, a time of predominantly vertical axis rotation similar to phase **II**, before reaching the present day "compressive" period of reverse-oblique faulting—phase **III**. The corresponding values for the dip and the strike of the rotating fault set are also shown. As the strike of the fault set rotates away from σ_1 (**I** $\rightarrow$ **II** in the plot), the dip flattens at first and then steepens as soon as the reverse slip field is reached (**II** $\rightarrow$ **III**).

3. Agreement with the observations

Our goal was to demonstrate how deformation in the WTR could have occured along a single set of faults, reactivated in middle Miocene time as block rotation began.

In agreement with the observations (Fig. 13), Fig. 15 displays the salient features predicted by the 3D BR model for the structural history of the WTR fault set. The original orientation of the fault set in the WTR domain must have been NNE striking, dipping $55^0 - 60^0$ to the West and slipping in a normal sense. Subsequently, the same fault set rotated away from the direction of maximum compression σ_1 and became strike-slip in style with a dip between 40^0 and 50^0. Finally, the fault set rotated into the E-W, high angle, reverse-oblique faults observed today. The results of our modeling show that along the rotation path, a single fault set went through three different faulting styles during its 75^0 clockwise rotation, while stress directions remained stationary with $S_v = \sigma_2$, σ_1 oriented $N20^0E$, and $\phi = constant$ at a value of 0.1.

These simplifying assumptions are not necessary. If we most accurately modeled the tectonic history of the WTR domain, we should have accounted for changes in stress directions that presumably took place between the Miocene and the Present. Evidence of this is found in studies of plate motion (Cox and Engebretson, 1985) that indicate a clockwise change in relative plate motion ~ 5 My ago. Incorporating this change would introduce an additional degree of freedom and allow a less restrained solution. The original orientation of faults could be even more N-S striking, and the amount of total rotation that could be achieved by one single set of faults would increase by an amount comparable to the change in plate motion.

The second constraining assumption, that of a constant ϕ stress history, mantains a strike-slip stress regime during the rotation history of the faults. This need not be the case. A change of stress regime might occur during the history of rotation of a fault set, and it could reverse the sense of rotation of blocks and faults or allow them to rotate in another direction.

Nevertheless, it is encouraging that with our simple 3D BR model and simple assumptions, we have been able to predict a sequence of structural phases

consistent with the known structural history of the WTR. This example demonstrates that one need not always invoke complex regional and local changes in the stress regime or erratic changes in plate motions to account for alternate periods of compression and extension. The geometry of each domain of fault sets determines the style of faulting that will occur there. The regional stress regime may remain stationary.

CONCLUSIONS

We have presented a generalized model of distributed deformation and block rotation that emphasizes faulting in 3 dimensions. The need for this model is dictated by the following observations:
(1) Reactivated faults are usually poorly oriented relative to the stress field.
(2) Obliquely slipping faults are found in many domains that have undergone rotation.
(3) These same faults change their faulting style through time.
We propose that mechanical constraints of friction and strength combined with the 3D Mohr circle and the kinematics of block rotation can explain these observations.

1. Block rotation: the cause of poorly oriented faults

According to the existing 2D BR model, rotation of blocks and faults are caused by contemporaneous slip on fault sets in adjacent domains. Based on fracture mechanics and friction criteria, the orientation of faults sets with respect to the direction of maximum compression σ_1 determines the sense of fault slip and thus the sense of rotation of the blocks in each domain. Consequently, faults that are initially in optimal orientations must rotate away from this optimal orientation in domains undergoing rotation. In this paper, we generalized these concepts into a 3D BR model.

With the 3D BR model, we are able to determine the range of orientations for faults that may slip as well as their style of faulting (i.e. rake). We can also determine the maximum amount of rotation blocks and faults may experience before a new set of faults may take over the deformation.

The results of our modeling show that the value of the ϕ parameter plays a key role in identifying those faults that may be reactivated and in determining their style of faulting. At low ϕ values, where σ_2 is close in magnitude to σ_3, faults may be reactivated even if very poorly oriented. Thus, in different domains at the same point in time or within the same domain through time, contrasting styles of faulting can occur. In a normal stress regime, both pure strike-slip and pure normal faulting styles can occur. In a reverse stress regime, both pure strike-slip and pure reverse faulting styles can occur. In a strike-slip stress regime, pure strike-slip, pure normal and pure reverse faulting styles can all occur. At high ϕ values, where σ_2 is closer to σ_1 in magnitude, faulting styles are limited to strike-slip and normal in both the normal and strike-slip stress regimes and only to reverse in the reverse stress regime.

When applied to the distributed deformation of Southern California, our model can explain the diverse faulting styles observed there by assuming a simple regional strike-slip stress regime with σ_1 oriented $N20^0E$, a low $\phi = 0.1$, and a coefficient of sliding friction of 0.4.

2. Change of faulting style with rotation

The importance of the ϕ parameter is also clearly demonstrated by the change in rake predicted by the 3D BR model as faults rotate in a stationary stress field. The results show that rake varies with rotation at low ϕ values, but

remains relatively constant at high values. By analyzing dip and strike of faults throughout rotation, we found surprising results. At low ϕ values in the reverse regime, originally poorly oriented faults may rotate about a vertical axis. On the other hand, at high ϕ values, poorly oriented faults may rotate unexpectedly about a vertical axis in the normal stress regime, and about a horizontal axis in the strike-slip stress regime. Therefore, for the general case of originally poorly oriented sets of faults, oblique axes of rotations are predicted by our model for all stress regimes.

We applied the 3D BR model to the complex history of faulting as documented in the Western Transverse Ranges of Southern California. The best model results indicate that for the WTR domain, a single set of originally NNE striking faults could have accommodated the deformation. Assuming a low ϕ strike-slip stress regime, a stationary $N20^0E$ directed maximum compressive stress, and a value of 0.4 for the coefficient of sliding friction, these faults were reactivated as normal faults at the beginning of the rotation period. Subsequently, the same faults became more NE striking, left-lateral strike-slip faults until they finally rotated into the present day "compressive" period of E-W striking reverse faults.

In spite of its simplifying assumptions, the our model provides clues to earlier geometries of faults for the WTR that are consistent with the geological, geophysical and paleomagnetic records.

We believe that block rotation is a fundamental process in regions of distributed deformation where poorly oriented faults are widespread. When applied to actual geologic situations, the model provides a powerful, yet simple tool to interpret the complex faulting histories and complex fault geometries that characterize regions of distributed deformation.

ACKNOWLEDGEMENTS

This study was supported by the Geodynamics Program of NASA, through grant no.NAG5-926 Mod.Amend01.

APPENDIX

1. Stress limits

A fault can slip and rotate when the Coulomb criterion for sliding is satisfied:

$$\tau_f = C_f + \mu_f \sigma_n \tag{1}$$

where τ is the shear stress on the fault plane, σ_n is the normal stress across it, C_f is the cohesion and μ_f is the coefficient of friction of the fault.

Prior to slip and rotation, it is necessary to check that the differential stress does not exceed the Coulomb fracture line:

$$\tau_0 = C_0 + \mu_0 \sigma_n \tag{2}$$

where C_0 is the cohesion and μ_0 is the coefficient of friction of the intact crust. This line defines the upper limit for the magnitude of the differential stress (R) in the earth's intact crust :

$$R = \frac{\sigma_1 - \sigma_3}{2} \leq R_{max} = \frac{1}{\sqrt{1+\mu_0^2}}[C_0 + \frac{\mu_0}{2}(\sigma_1 + \sigma_3)] \tag{3}$$

Furthermore, it is necessary to ensure that:

$$\sigma_3 \geq 0 \tag{4}$$

because the crust cannot support tension.

2. Stress model and stress paths

The normal (σ_n) and shear (τ) stresses across a plane are computed according to the following relations (Jaeger and Cook, 1969):

$$\sigma_n = \alpha_1^2 \sigma_1 + \alpha_2^2 \sigma_2 + \alpha_3^2 \sigma_3 \tag{5}$$

$$\tau^2 = \alpha_1^2 \sigma_1^2 + \alpha_2^2 \sigma_2^2 + \alpha_3^2 \sigma_3^2 - \sigma_n^2 \tag{6}$$

where $\alpha_1, \alpha_2, \alpha_3$ are the direction cosines of the pole (fault normal) with respect to the principal stress axes, $\sigma_1, \sigma_2, \sigma_3$.

As principal stress magnitudes change to satisfy equation (1), the initial value (σ_n, τ) on a given fault plane will change to a new value (σ_n', τ'). The sequence of (σ_n', τ') described by the pole is computed with α_1, α_2, $\alpha_3 = constant$, because during these stress changes and before any rotation event occurs, the fault plane itself remains fixed in stress space.

This sequence of (σ_n', τ') will be referred to as the stress path of a fault. It depends on the stress history chosen and on the initial conditions (σ_n, τ, σ_1, σ_2, σ_3, α_1, α_2, α_3).

As explained in the text, this paper considers three stress regimes in which one of the principal stress axis is always assumed vertical (S_v) and the stresses are assumed to change according to a $\phi = (\sigma_2' - \sigma_3')/(\sigma_1' - \sigma_3') = constant$ model. For each stress regime, the stress path of a fault is computed as follows:

a. NORMAL STRESS REGIME ($S_v = \sigma_1$)

$$\sigma_1' = \sigma_1 = constant \tag{7}$$

$$\sigma_2' = \sigma_2 - r_N \Delta\sigma \tag{8}$$

$$\sigma_3' = \sigma_3 - \Delta\sigma, \tag{9}$$

where

$$r_N = \frac{\sigma_1 - \sigma_2}{\sigma_1 - \sigma_3}. \tag{10}$$

b. REVERSE STRESS REGIME ($S_v = \sigma_3$)

$$\sigma_1' = \sigma_1 + \Delta\sigma \tag{11}$$

$$\sigma_2' = \sigma_2 + r_R \Delta\sigma \tag{12}$$

$$\sigma_3' = \sigma_3 = constant \tag{13}$$

where

$$r_R = \frac{\sigma_2 - \sigma_3}{\sigma_1 - \sigma_3} \tag{14}$$

c. STRIKE-SLIP STRESS REGIME ($S_v = \sigma_2$)

$$\sigma_1' = \sigma_1 + \Delta\sigma \tag{15}$$

$$\sigma_2' = \sigma_2 = constant \tag{16}$$

$$\sigma_3' = \sigma_3 - r_S \Delta\sigma \tag{17}$$

where

$$r_S = \frac{\sigma_2 - \sigma_3}{\sigma_1 - \sigma_2} \tag{18}$$

Substituting the values for σ_i' into equations (5) and (6), the stress paths that result from the above models are given by the following equations with $\Delta\sigma$ as a parameter:

$$\sigma_n' = \sigma_n + a\Delta\sigma \tag{19}$$

$$\tau'^2 = \tau^2 + b\Delta\sigma + c(\Delta\sigma)^2 \tag{20}$$

where $\sigma_1, \sigma_2, \sigma_3, \tau, \sigma_n$ are known initial values and $\alpha_1, \alpha_2, \alpha_3$ are the constant direction cosines of the fault normal. The coefficients a, b and c assume different values depending on the stress regime considered (see Table A1).

	Coefficients		
Stress Regime	*a*	*b*	*c*
normal	$-(\alpha_3^2 + r_N\alpha_2^2)$	$-2[r_N\alpha_2^2(\sigma_2 - \sigma_n) + \alpha_3^2(\sigma_3 - \sigma_n)]$	$(1 - r_N)^2\alpha_2^2\alpha_3^2 + (\alpha_3^2 + r_N^2\alpha_2^2)\alpha_1^2$
reverse	$\alpha_1^2 + r_R\alpha_2^2$	$2[\alpha_1^2(\sigma_1 - \sigma_n) + r_R\alpha_2^2(\sigma_2 - \sigma_n)]$	$(1 - r_R)^2\alpha_1^2\alpha_2^2 + (\alpha_1^2 + r_R^2\alpha_2^2)\alpha_3^2$
strike-slip	$\alpha_1^2 - r_S\alpha_3^2$	$2[\alpha_1^2(\sigma_1 - \sigma_n) - r_S\alpha_3^2(\sigma_3 - \sigma_n)]$	$\alpha_1^2 + r_S^2\alpha_3^2 - a^2$

Table A1. *a, b and c are coefficients required to calculate the stress path of a fault. They depend on the orientation of the faults (α_1, α_2, α_3), the assumed stress model (r_N, r_R, r_S) and the initial values of σ_1, σ_2 and σ_3.*

Replacing $\Delta\sigma$ from (19) into (20), we get an explicit equation for the stress path

$$a^2\tau'^2 = A\sigma_n'^2 + B\sigma_n' + C, \tag{21}$$

where

$$A = c \tag{22}$$

$$B = ab - 2c\sigma_n \tag{23}$$

$$C = a^2\tau^2 - ab\sigma_n + c\sigma_n^2 \tag{24}$$

By combining equation(21) and equation(1), we obtain the coordinates σ_n', τ' of the intersection between the pole's stress path and the Coulomb sliding line. There the fault plane can slip and rotate.

3. Rotation of fault planes

Consider a normal to a fault plane with unitary vector direction cosines α_1, α_2, α_3. Once the shear stress τ across the fault plane satisfies equation (1), the fault plane will slip and rotate in the direction of the resolved shear stress, represented by the unitary vector $\tilde{\tau}$. [1] The nature of this rotation is better understood in Fig. A1, where the horizontal plane represents the fault before rotation and $\tilde{r}$ is its unit normal vector (same direction as $\vec{\sigma}_n$).

Given the coordinates $\alpha_1, \alpha_2, \alpha_3$ of the normal to the fault $\tilde{r}$ and the coordinates of the total stress vector ($\vec{\sigma}$) across it

$$[\vec{\sigma}]_1 = \alpha_1\sigma_1 \tag{25}$$

$$[\vec{\sigma}]_2 = \alpha_2\sigma_2 \tag{26}$$

[1] A tilde will denote a unitary vector

$$[\vec{\sigma}]_3 = \alpha_3\sigma_3, \tag{27}$$

we can compute the coordinates of vectors $\tilde{n}$, $\tilde{r}$ and $\tilde{\tau}$. In order to compute $\tilde{n}$ we first compute vector $\vec{n} = \tilde{r} \times \vec{\sigma}$ with coordinates:

$$n_1 = \alpha_2\alpha_3(\sigma_3 - \sigma_2) \tag{28}$$

$$n_2 = \alpha_1\alpha_3(\sigma_1 - \sigma_3) \tag{29}$$

$$n_3 = \alpha_1\alpha_2(\sigma_2 - \sigma_1) \tag{30}$$

Vector $\tilde{n}$ is then simply $\vec{n}/|\vec{n}|$. Similarly, $\vec{\tau}=\tilde{n} \times \tilde{r}$ and has coordinates:

$$\tau_1 = \alpha_1\{\alpha_3^2(\sigma_1 - \sigma_3) - \alpha_2^2(\sigma_2 - \sigma_1)\} \tag{31}$$

$$\tau_2 = \alpha_2\{\alpha_1^2(\sigma_2 - \sigma_1) - \alpha_3^2(\sigma_3 - \sigma_2)\} \tag{32}$$

$$\tau_3 = \alpha_3\{\alpha_2^2(\sigma_3 - \sigma_2) - \alpha_1^2(\sigma_1 - \sigma_3)\} \tag{33}$$

The direction cosines of the rotated plane will be the coordinates of the vector $\tilde{r}'$. Therefore, they must satisfy the following 3 equations:

$$\tilde{r}' \cdot \tilde{n} = 0 \Longrightarrow \alpha_1' n_1 + \alpha_2' n_2 + \alpha_3' n_3 = 0 \tag{34}$$

$$\tilde{r}' \cdot \tilde{r} = \cos\delta\rho \Longrightarrow \alpha_1'\alpha_1 + \alpha_2'\alpha_2 + \alpha_3'\alpha_3 = \cos\delta\rho \tag{35}$$

$$\tilde{r}' \cdot \tilde{\tau} = \tilde{r}' \cdot \vec{\tau}/|\vec{\tau}| = \sin\delta\rho \Longrightarrow \alpha_1'\tau_1 + \alpha_2'\tau_2 + \alpha_3'\tau_3 = \sin\delta\rho \cdot |\vec{\tau}| \tag{36}$$

After rotation has occured, principal stresses will drop and Mohr circles should "shrink". The newly computed values of the rotated fault plane direction cosines $(\alpha_1', \alpha_2', \alpha_3')$ define a new stress path, along which the pole must move as the stresses change (after each rotation we can choose a different model for stress changes). No direct relationship exists yet between the amount of stress drop and the amount of rotation. Nonetheless, whatever the stress drop, the new pole must move along its stress path. Since the rotation path is fully defined by the intersection between the stress path and the sliding line, it is not necessary to know the stress drop (that is, how far the pole will move along its new path) to estimate the next rotation event.

REFERENCES

Anderson, E.M., 1951, The dynamics of faulting. Oliver and Boyd, Edinburgh, 206pp

Angelier, J., Colletta, B. and Anderson R.E., 1985, Neogene paleostress changes in the Basin and Range: a case study at Hoover Dam, Nevada-Arizona, G.S.A.Bull, **96**, 347-361

Bott, M.H.P., 1959, The mechanics of oblique slip faulting. Geol.Mag.,**XCVI**, 2

Brown, L. and Golombek, P., 1986, Block rotations in the Rio Grande Rift, New Mexico, Tectonics, **5**, 3, 423-438

Carter, J.N., Luyendyk, B.P. and Terres, R.R., 1987, Neogene clockwise tectonic rotation of the eastern Transverse Ranges, California, suggested by paleomagnetic vectors, G.S.A.Bull, **98**, 199-206

Cox, A. and Engebretson, D., 1985, Change in plate motion of Pacific plate at 5Myr BP. Nature,**313**, 472-474

Dokka R. K., 1989, The Mojave extensional belt of Southern California, Tectonics, **8**, 2, 363-390

Estevez, R., Scotti, O. and Nur, A., 1987, Block rotation in 3D., Stanford Rock Physics Project, Unpublished manuscript

Freund, R., 1970, Rotation of strike-slip faults in Sistan, Southeast Iran. J.Geol.,**78**, 188-200

Freund, R., 1971, The Hope fault, a strike-slip fault in New Zealand, N.Z.Geol.Surv., Bull., **86**, 49pp.

Freund, R. , 1974, Kinematics of transform and transcurrent faults. Tectonophysics,**21**, 93-134

Garfunkel, Z., 1974, Model for the late Cenozoic tectonic history of the Mojave desert, California, and for its relation to adjacent regions. G.S.A.Bull, **85**, 1931-1944

Handin, J., 1969, On the Coulomb-Mohr failure criterion. J.G.R.,**74**, 22

Hornafius, J.S., Luyendyk, B.P., Terres, R.R. and Kamerling, M.J., 1986, Timing and extent of Neogene tectonic rotation in the western Transverse Ranges, California, G.S.A.Bull, **97**, 1476-1487

Hudson M.R. and Geissman J.W., Paleomagnetic and structural evidencefor middle Tertiary counterclockwise block rotation in the Dixie velley region,west-central Nevada, 1987, Geology **15**, 638-642

Jackson J.A. and White, N.J., 1989, Normal faulting in the upper continental crust: observations from regions of active extension. Journan of Struct.

Geol., **11**, 1/2, 15-36

Jaeger, J.C. and Cook, N.G.W., 1969, Fundamentals of rock mechanics. Methuen and Co.Ltd, London, 515pp

Jaeger, J.C. and Rosengren, K.J., 1969, Friction and sliding of Joints. Proc. Aust. Inst. Min. Met.,**229**, 93-104

Jennings, C.W, 1975, Fault Map of California, Calif.Div. of Mines and Geology

Jones, L.M., 1988, Focal mechanisms and the state of stress on the San Andreas fault in Southern California. J.G.R.,**93**, B8, 8869-8891

Kamerling, M.J. and Luyendyk, B.P., 1985, Paleomagnetism and Neogene Tectonics of the Northern Channel Islands, California. JGR,**90**, B14, 12, 485-12, 502

Kissel C., Laj C. and Mazaud A., 1986, First paleomagnetic results from Neogene formations in Evia, Skyros and the Volos region and the deformationof central Aegea., Geophy. Res. Lett., **13**, 13, 1446-1449

Lee, W.H.K., Yerkes, R.F. and Simirenko, M., 1979, Recent earthquake activity and focal mechanisms in the Western Transverse Ranges, California. in U.S.Geological Survey, Map MF-1032

Li Y., Geissman J., Nur A., Ron H. and Huang Q., 1990 Counterclockwise block rotation in the North Nevada Rift region: paleomagnetic evidence, Geology, **18**, 79-82

Luyendyk, B.P., Kamerling, M.J. and Terres, R.R., 1980 Geometric model for Neogene crustal rotations in Southern California. GSA Bull,**91**, 211-217

Luyendyk, B.P., Kamerling, M.J., Terres, R.R. and Hornafius J.S., 1985, Simple shear of Southern California during Neogene times suggested by paleomagnetic declinations. J.G.R.,**90**, B14, 12, 454-12, 466

Luyendyk, B.P. and Hornafius, J.S., 1987, Neogene crustal rotations, fault slip and basin development in Southern california, in Ingersoll R.V. and Ernst W. G. (eds.), Rubey Vol VI, Cenozoic basin development of coastal California,, 259

McKenzie, D.P., 1969, The relation between fault plane solutions for earthquakes and the directions of principal stresses. B.S.S.A,**59**, 2, 591-601

Jackson J. and McKenzie, D.P., 1983, The geometrical evolution of normal fault systems, J. struct. Geol.,**5**, 471-482

Jackson J. and McKenzie, D.P., 1984, Active tectonics of the Alpine-Himalayan Belt between western Turkey and Pakistan, Goephys. J. R. astr. Soc.,**77**,185-264

Molnar, P., 1988, Continental tectonics in the aftermath of plate tectonics. Nature, **335**, 131-137

Namson, J. and Davis, T., 1988, Structural transect of the western Transverse Ranges, California: Implications for lithospheric kinematics and seismic risk evaluation, Geology, **16**, 675-679

Nur, A., Ron, H. and Scotti, O., 1986, Fault mechanics and the kinematics of block rotations. Geology, **14**, 746-749

Pavlides, S.B., Kondopoulou, D.P., Kilias, A.A. and Westphal M., 1988, Complex rotational deformations in the Serbo-Macedonian massif (north Greece): structural and paleomagnetic evidence, Tectonophysics, **145**, 329-335

Powell, R.E., 1982, Crystalline basement terranes in the South-Eastern Transverse ranges , Southern California. in Geological excursion in the Transverse Ranges, edited by GSA Cordillera section, pp109-151

Ransome, F.L., Emmons, W.H. and Garrey, G.H., 1910, Geology and ore deposit of the Bullfrog district, Nevada. U.S.G.S. Bull., **407**, 1-130

Ron, H., Freund, R., Garfunkel, Z. and Nur, A., 1984, Block-rotation by strike-slip faulting: structural and paleomagnetic evidence. J. Geophy. Res.,**89**, 6256-6270

Ron, H., Nur, A., Aydin, A., 1989, Stress field rotation or block rotation: an example from the Lake Mead fault system, submitted to Tectonics

Sauber, J.W., Tatcher, W. and Solomon, S.C., 1986, Geodetic measurements of deformation in the central Mojave Desert, California. J.Geophy.Res., **91**, 12.683-12.693

Terres, R.R. and Luyendyk, B.P., 1985, Neogene tectonic rotation of the San Gabriel region, California suggested by paleomagnetic vectors, J.G.R., **90**, B14, 12, 467-12, 484

Yeats R.S., 1987, Changing tectonic styles in Cenozoic basins of Southern California, in Ingersoll R.V. and Ernst W. G. (eds.), Rubey Vol VI, Cenozoic basin development of coastal California,, 259

Yerkes, R.F. and Lee, W.H., 1979a, Late quaternary deformation in the West Transverse ranges, California,U.S.Geol.Survey Circular. **799-B**, 27-37

Yerkes, R.F. and Lee, W.H, 1979b Map showing faults and fault activity and epicenters, focal depths and focal mechanisms for 1970-1975 earthquakes, Western transverse Ranges, California. U.S.Geol.Survey Misc.Field Studies, Map MF-1032

Yerkes, R.F. et al., 1981, Seismotectonic setting of the Santa Barbara channel area, Southern California. Map MF-1169

Zoback, M.D. and Healy, J.H., 1984, Friction, faulting, and << in situ >> stress, Annales Geophysicae, **2**, 6, 689-698

Zoback, M.D. et al., 1987, New evidence on the state of stress of the San Andreas fault system, Science, **238**, 1105-1111

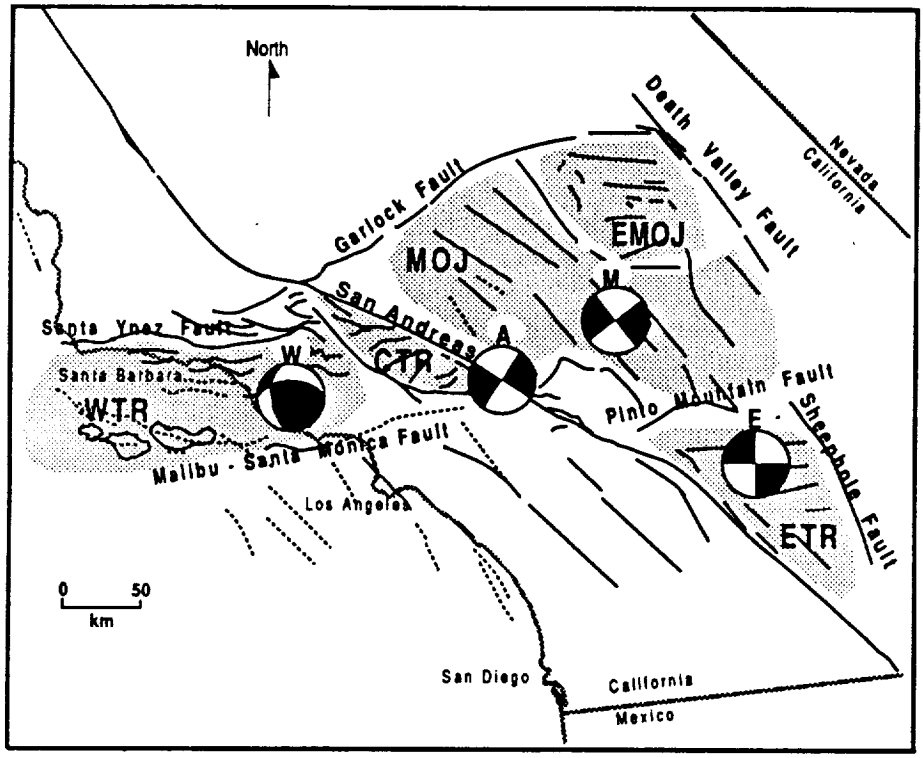

Fig. 1 **Structural domains in Southern California.** *Sub-parallel sets of faults (Quaternary in Age) of different orientations define structural domains: Mojave (MOJ) and East Mojave (EMOJ), West (WTR), Central (CTR) and East Transverse Ranges (ETR). Domains are separated by throughgoing boundary faults such as the San Andreas, Santa Ynez, and Garlock faults (base map adapted from Jennings, 1975). Representative fault plane solutions (W, E and M) for three domains and for the San Andreas fault (A) are also shown.*

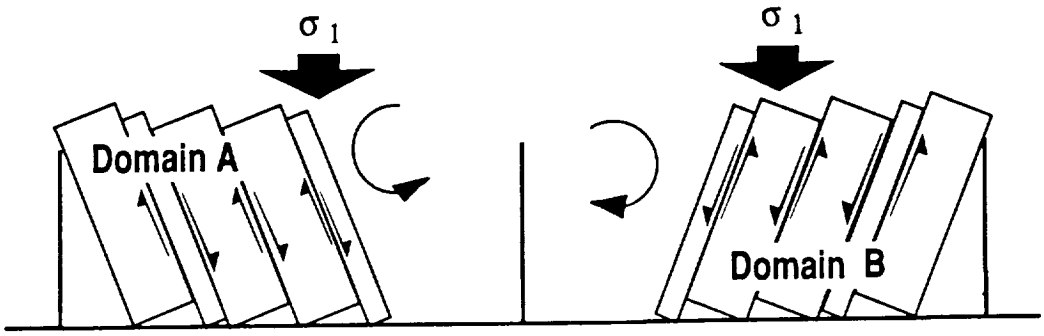

Fig. 2 **Kinematics of block rotation.** *Blocks (books) of different orientations abut against boundary faults (shelf and book-holders). The orientation of the blocks with respect to the direction of maximum compression (in this case gravity) controls the sense of slip and therefore the sense of rotation of blocks.*

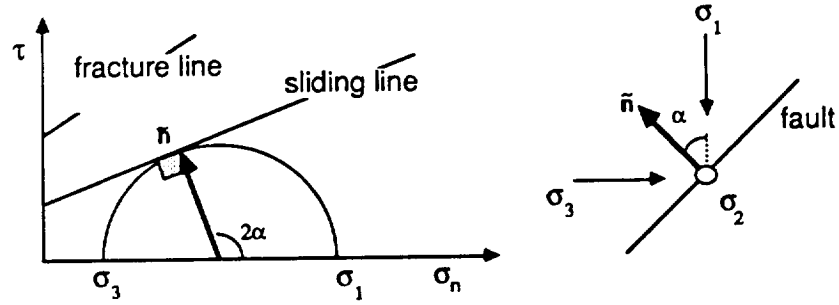

Fig. 3 **Optimally oriented fault.** *According to traditional friction models (Zoback and Healy, 1984), active faults are generally optimally orientd in the principal stress axis. Therefore, when plotted on the Mohr circle, optimally oriented faults should be represented by a $\sigma_1 - \sigma_3$ circle tangent to the sliding line, with the intermediate stress σ_2 contained in the plane of the fault.*

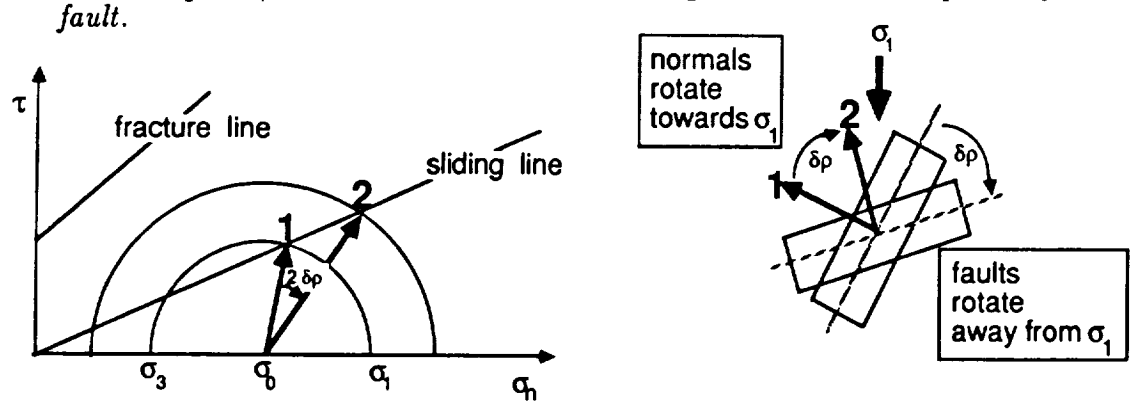

Fig. 4 **Mechanics of block rotation.** *The 2D Mohr circles show values of σ_n and τ required for the fault to slip, when its fault normal is at point 1, and when the fault rotated to a point 2, closer to the σ_1 direction. The lines represent the Coulomb criterion for sliding along preexisting faults and the Coulomb criterion for fracturing an intact rock mass. As illustrated in the sketch to the right, faults rotate away from σ_1. Therefore, normals to faults (poles to fault planes) will rotate towards σ_1, on a Mohr circle.*

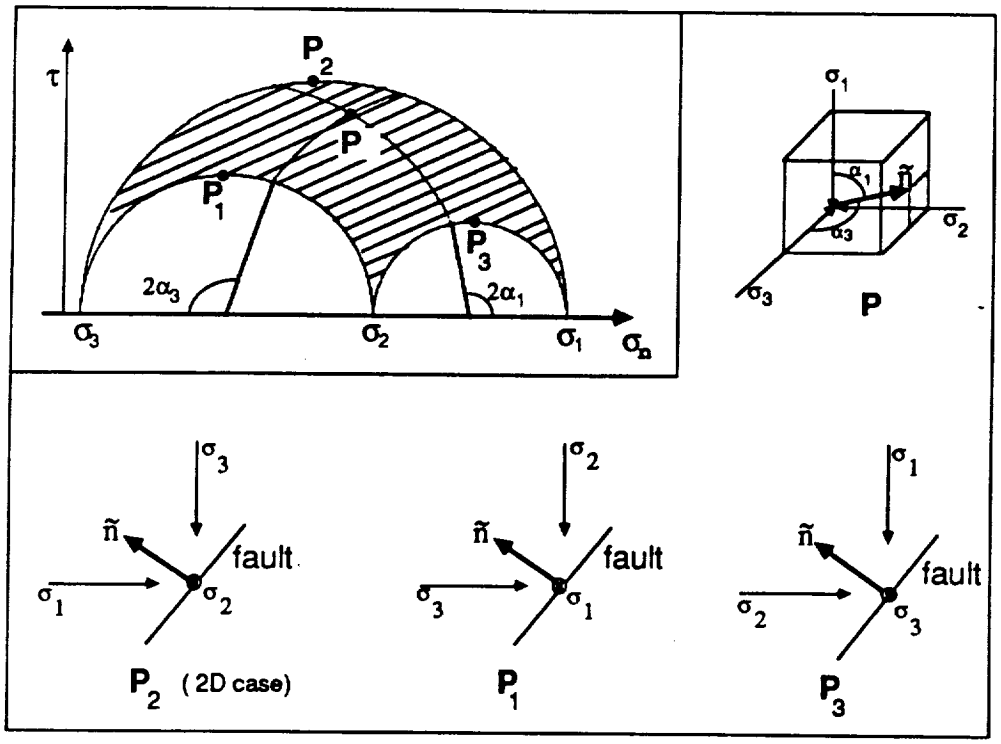

Fig. 5a The 3D Mohr circle is a 3-dimensional construction on a 2-dimensional $\sigma_n - \tau$ plane. Any point in the shaded region represents the orientation of a fault plane in space. For example, α_1 and α_3 are the direction cosines of a pole (P) relative to the σ_1 and σ_3 directions respectively. Three specific cases are shown: pole (P_2) plotting on the $\sigma_1 - \sigma_3$ circle with the σ_2 direction contained in its fault plane, identical to the 2D case; pole (P_1) plotting on the $\sigma_2 - \sigma_3$ circle, with the σ_1 direction in its fault plane and pole (P_3) plotting on the $\sigma_1 - \sigma_2$ circle, with the σ_3 direction in the fault plane.

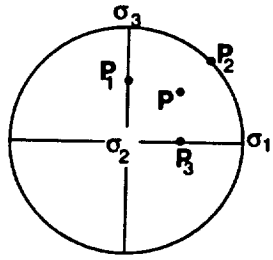

Fig. 5b Poles P, P_1, P_2 and P_3 of Fig. 5a are plotted in a lower hemisphere Wulff stereo projection. This is another way of plotting the orientation of poles to faults in a 3D space.

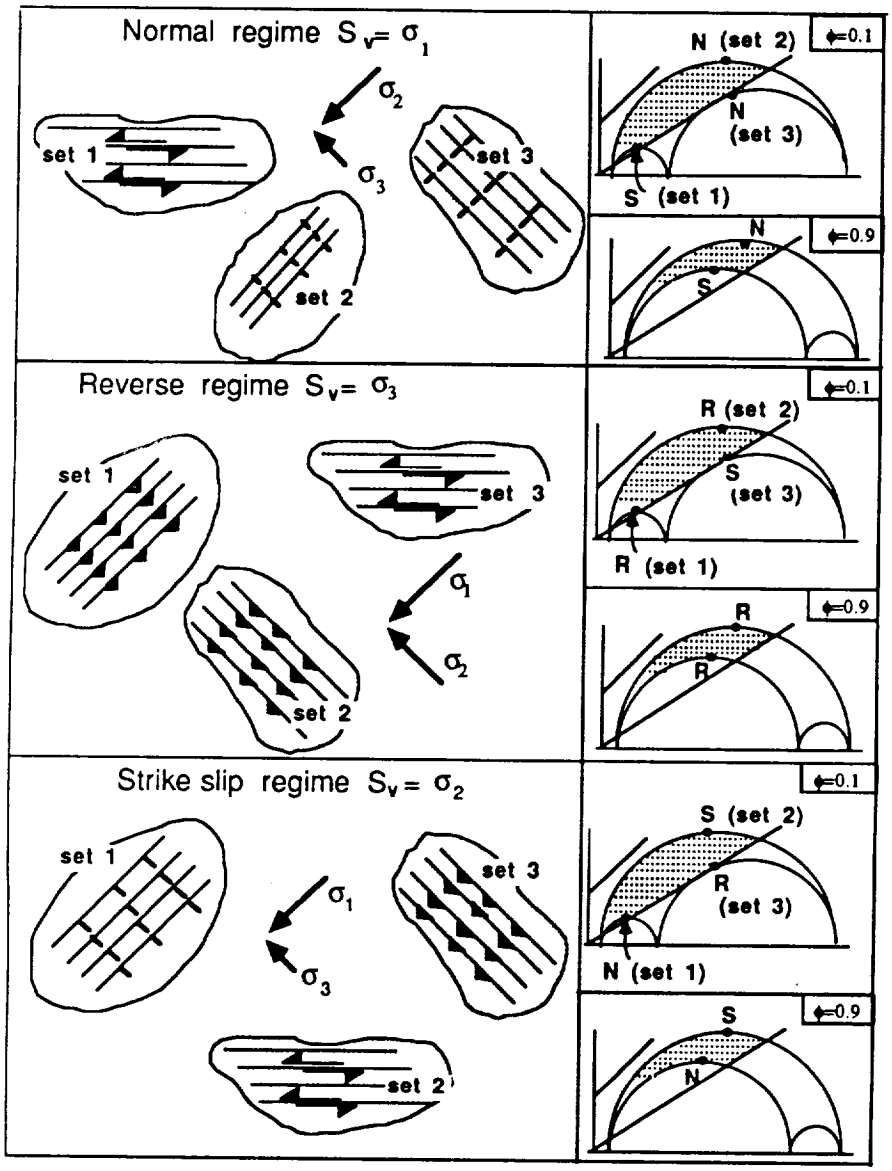

Fig. 6 **Mohr circle, friction criteria and faulting styles.** *Different faulting styles (N = pure normal, R = pure reverse, S = pure strike-slip) may occur in a region of distributed deformation. It depends on the orientation of the fault sets, the tectonic stress regime and the stress ratio ϕ as well as on the material parameters. Here we consider three sets of faults subjected to the three tectonic stress regimes (assuming 1.0 and .6 for the fracture and sliding coefficeints respectively): set 2 which contains the σ_2 direction in its plane (the 2D case), set 1 which contains the σ_1 direction in its plane and, set 3 which contains the σ_3 direction in its plane.*

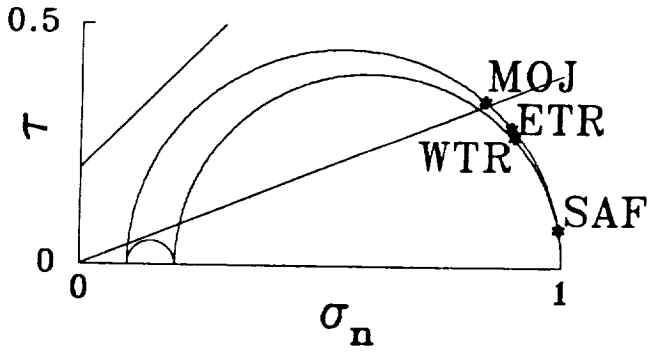

Fig. 7 Representative fault planes shown in Fig. 1 are plotted on a 3D Mohr circle (normalized by σ_1). A slope of 0.4 for the sliding line, a value of $\phi = 0.1$ for the stress ratio and a regional strike slip stress regime with σ_1 $N20^0E$ directed are required to slip faults in the different domains. Notice that the San Andreas fault (SAF), a major throughgoing boundary fault, cannot slip in accordance with friction criteria assumed in this model.

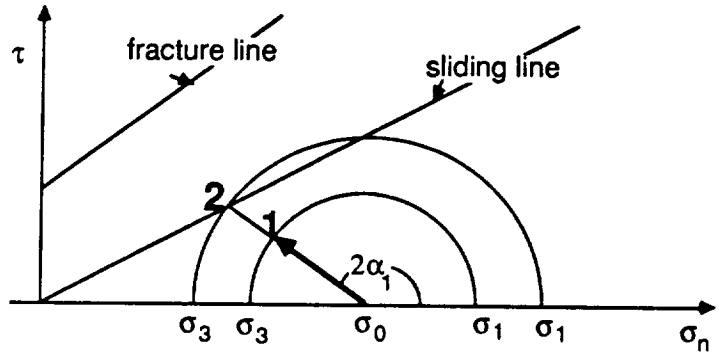

Fig. 8a. Assume a set of faults exists in a domain with an orientation α_1 to the σ_1 direction. The σ_2 direction is contained in the fault plane. Stress magnitudes must change (1 → 2) to allow sliding on the fault set. Assume that this change takes place by keeping the mean stress σ_0 constant.

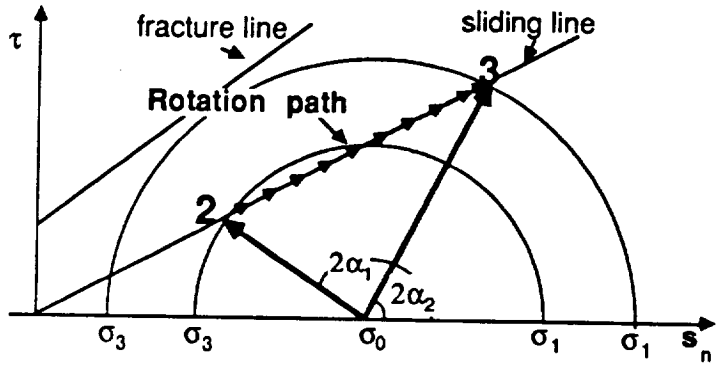

Fig. 8b. **The Rotation Path**: *At point 2 there is sufficient shear stress to overcome friction. The faults of a set slip and rotate. On the Mohr circle poles to faults are plotted (see Fig. 4). Thus, as rotation proceeds, stress magnitudes change and the poles plot closer and closer to σ_1 tracing a rotation path from 2 to 3 along the sliding line.*

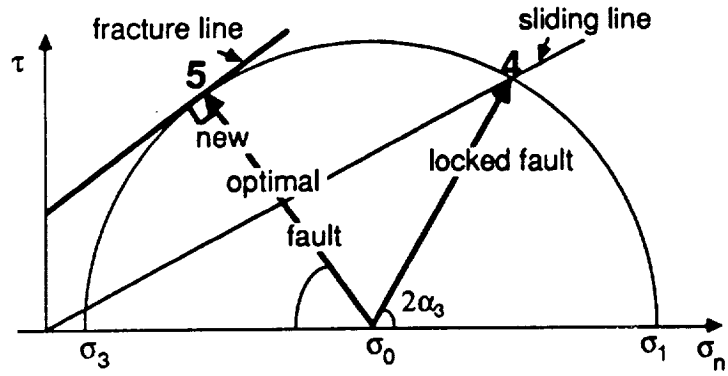

Fig. 8c At point 4 rotation along this set of faults ceases once stress magnitudes have reached the fracture line. Therefore a new, more optimally oriented set of faults forms, point 5, and the old set remains locked into an orientation α_3 relative to σ_1. In 2D, only fault orientations with the σ_2 direction in their plane can be modeled. After each rotation step, faults plot on the $\sigma_1 - \sigma_3$ circle. This results in only one rotation path and a constant fault behaviour.

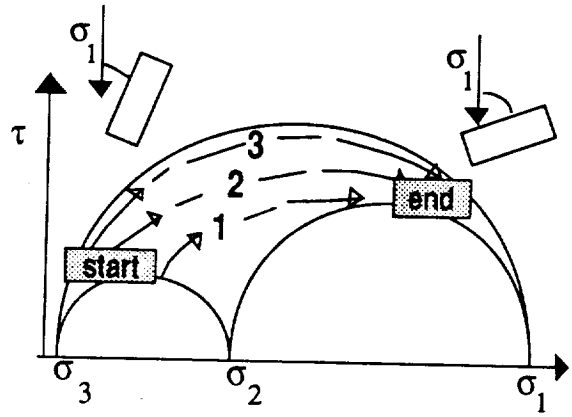

Fig. 9. In 3D there are many rotation paths. In this paper we consider three specific paths. They all start close to the σ_3 direction but rotation path for pole 1 starts close to the $\sigma_2 - \sigma_3$ circle, rotation path for pole 3 starts close to the $\sigma_1 - \sigma_3$ circle, rotation path for pole 2 starts at an intermediate position between the two. Rotation paths shown in this figure and Fig. 11 are plotted on graphs normalized by the magnitude of σ_1. The stress ratio ϕ remains constant throughout the rotation history of a fault set. Thus rotation paths will appear as curved lines.

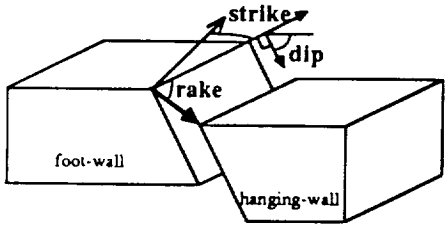

Fig. 10: The orientation of a fault set is given by the strike, or the azimuth of the fault with respect to a reference direction, and the dip, or the angle between the fault plane and the horizontal plane (0^0 = horizontal; 90^0 = vertical). The style of faulting is determined by the rake, or the angle between the direction of fault slip and the horizontal ($+90^0$ = pure normal; 0^0 = pure strike – slip; -90^0 = pure reverse).

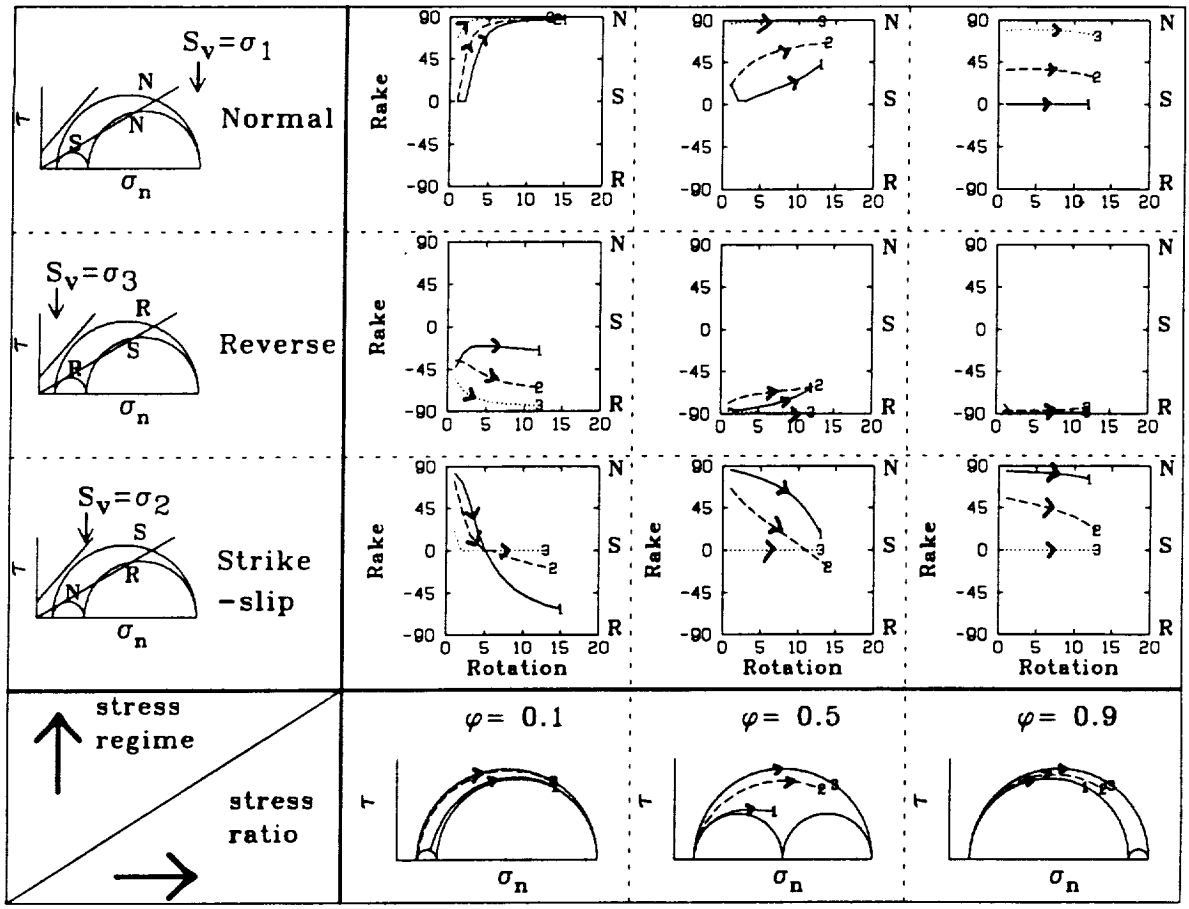

*Fig. 11 Cross-plot of faulting styles for different stress regimes and ϕ ratios. The faulting style evolves along various rotation paths in plots of rake vs. rotation. Strike-slip fault styles (**S**) are at 0^0, normal (**N**) styles are at 90^0, and reverse (**R**) styles are at -90^0. Fig. 9's case 1 plots with a solid line, case 2 with dashes, and case 3 with dots. Variations in rake with rotation are sensitive to σ_2. Low ϕ values change the modeled rake dramatically while high values leave it largely unchanged along the rotation paths.*

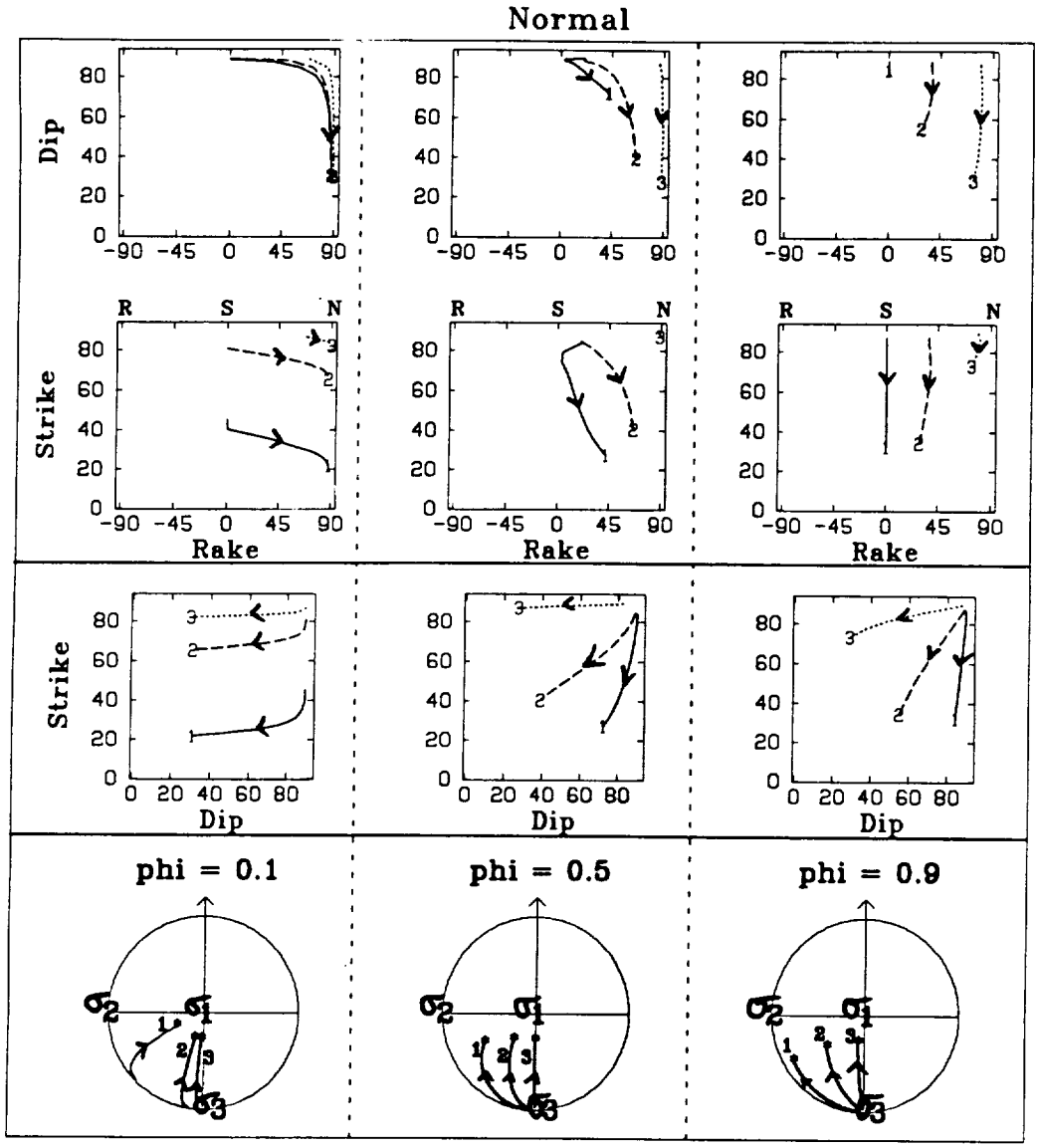

Fig. 12a Rake versus Dip, Rake versus Strike and Dip versus Strike are plotted for the three rotation paths (1, 2, 3) at different values of the stress ratio ϕ. The arrows indicate the sense of rotation. Wulff stereo-projections for the three rotation paths are shown, for reference, at the bottom of each figure.

Normal stress regime, $S_v = \sigma_1$. *The flattening of the dip decreases with increasing stress ratio. The rake changes from strike-slip to normal at low stress ratios ($\phi = 0.1$) but remains constant at the initial value at high stress ratios. This is accompanied by an increase in vertical axis rotation with increasing stress ratio (see rotation paths 1 and 2): the strike is relatively constant at low stress ratios but changes considerably at high ratios (σ_3 is at strike= 0^0).*

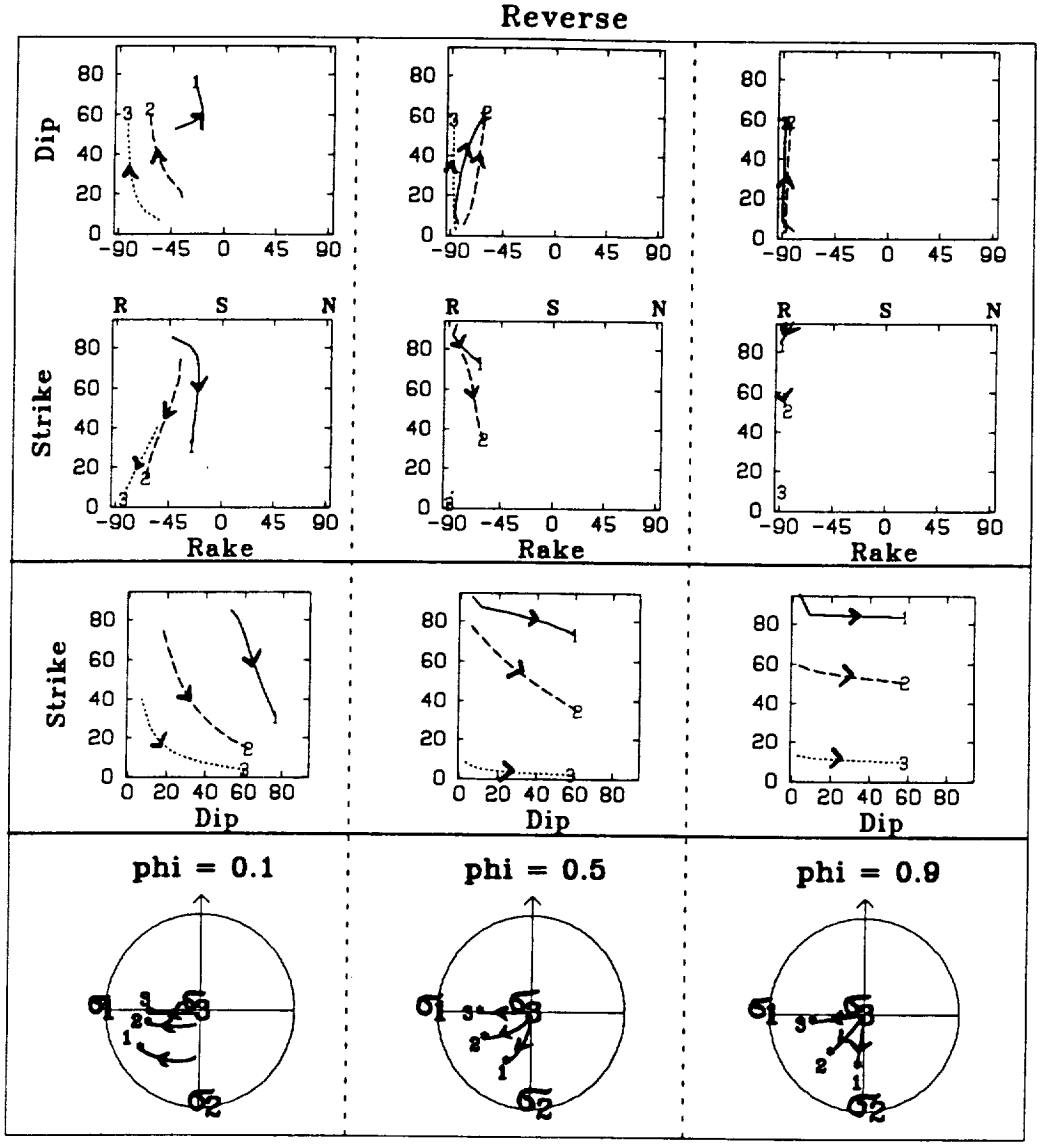

Fig. 12b **Reverse stress regime,** $S_v = \sigma_3$. *The dip steepens throughout rotation for all fault planes at all stress ratios. The rake changes from oblique-strike-slip to oblique-reverse-slip (rotation path 1) or to strike-slip (rotation path 2) at low stress ratios but at intermediate and high stress ratios the rake is reverse along all rotation paths. This is accompanied by a vertical axis rotation at low* ϕ *values (see rotation paths 1 and 2) where the strike changes considerably. At higher stress ratios, rotations occur predominantly about a horizontal axis (*σ_2 *is at strike=* 0^0*).*

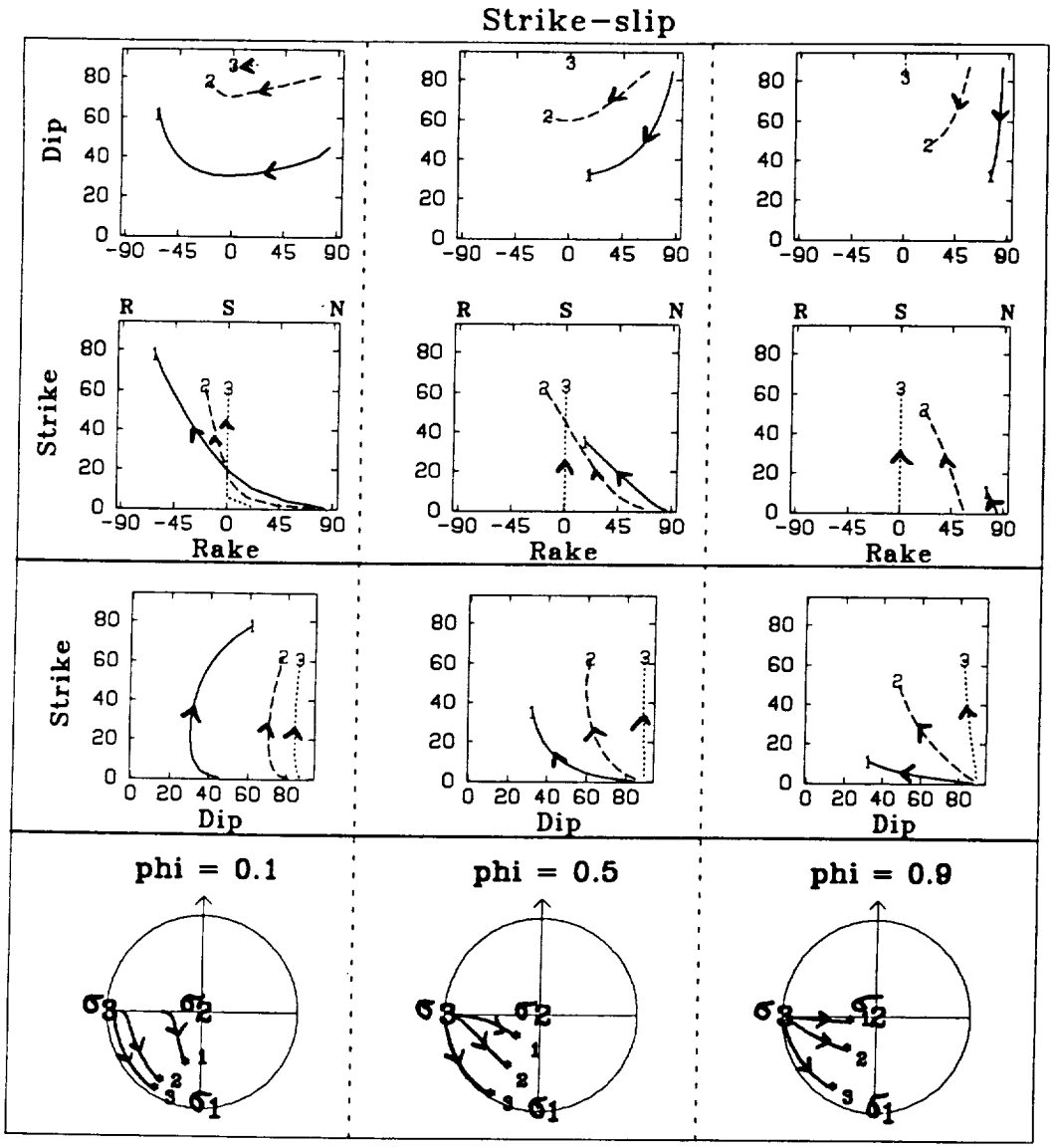

Fig. 12c **Strike slip stress regime,** $S_v = \sigma_2$. *As the rake goes from normal, through strike-slip and then to reverse, the dip of the fault plane flattens at first and then steepens at low stress ratios* ($\phi = 0.1$). *At higher stress ratios rotation stops before the reverse field is reached. The strike change is greater than the dip change, producing predominant vertical axis rotations in most cases* (σ_1 *is at strike*$= 0$). *An exception to this is rotation path for pole 1 at* $\phi = 0.9$*: the strike does not change, only the dip and therefore a purely horizontal axis rotation can occur in a strike-slip stress regime.*

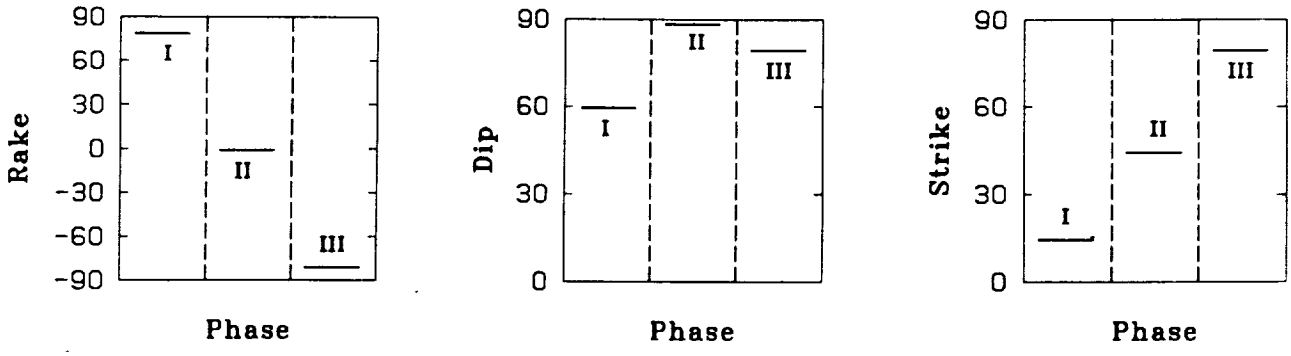

Fig. 13 Observed and inferred rake, dip and strike of the WTR fault set since Miocene times. Based on structural, geological and paleomagnetic data as discussed in the text. σ_1 si assumed at $N20^0E$ and is at strike= 0^0 on the plot.

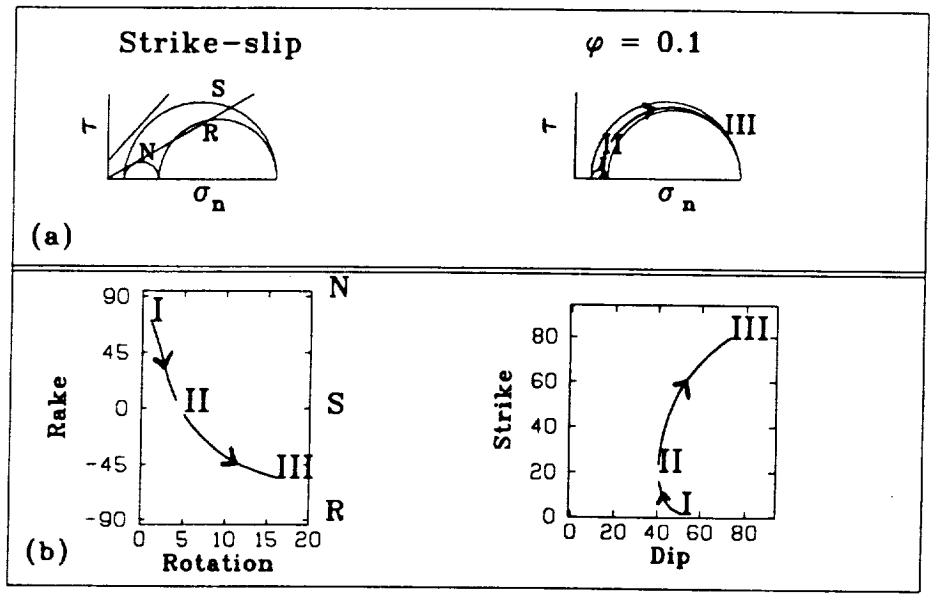

Fig. 14 **Modeling 3D fault rotation in the West Transverse Ranges.** *(a) The rotation path predicted by the 3D BR model, assuming, as in Fig. 7, a strike slip stress regime with the maximum principal stress direction σ_1 $N20^0E$, a coefficient of friction $\mu_f = 0.4$, and a stress history with a constant stress ratio $\phi = 0.1$. (b) According to the 3D BR model, a single set of rotating faults may have accommodated the deformation of the WTR domain. The model predicts, in accordance with observations summarized in Fig. 13, three different phases of faulting styles since rotation began: normal-oblique faulting* **(I)** $\rightarrow$ *strike-slip faulting* **(II)** $\rightarrow$ *high angle reverse-oblique faulting* **(III)**.

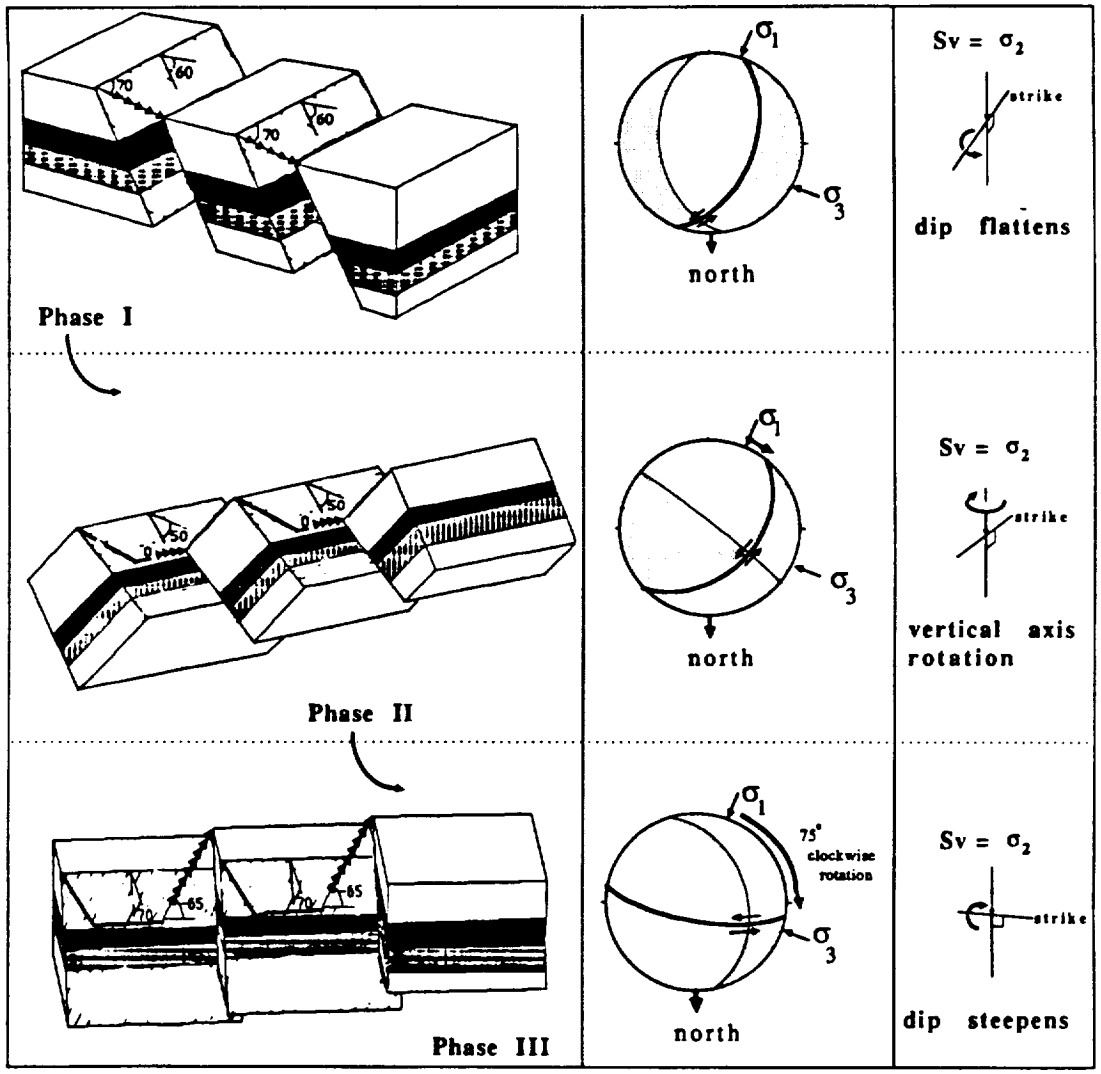

Fig. 145 The evolution of the rake, the dip, and the strike of the faults of the WTR through time. Each phase may be better visualized with idealized block diagrams and focal plane solutions (lower hemisphere projections). The sketches in the right column show the dominant axis of rotation, where S_v refers to the principal vertical stress axis and the strike of the fault is shown. When the strike of the fault is almost parallel to σ_1—phase **I** *—the faults move in a normal-oblique (***rake= +70***) sense. When none of the principal stresses are parallel to the strike of the faults—phase* **II***—the faults move in a strike-slip sense (***rake= 0***). Finally, when the strike of the fault becomes parallel with the σ_3 direction—phase* **III***— the faults move in a reverse-oblique sense (***rake= -65***).*

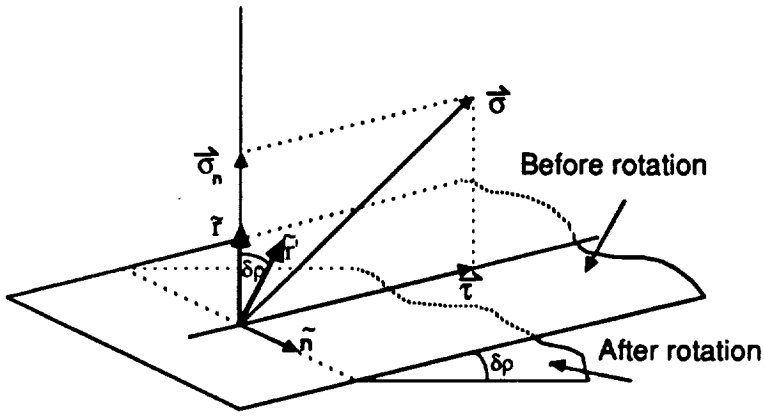

Fig. A1: **Rotation of Fault Planes.** *The horizontal plane, with its normal vector* $\tilde{\mathbf{r}}$*, represents the initial orientation of the fault. During rotation, the normal* $\tilde{\mathbf{r}}$ *will rotate through an angle* $\delta\rho$ *within the plane (normal* $\tilde{\mathbf{n}}$*) that contains* $\vec{\sigma}_\mathbf{n}$*,* $\tilde{\mathbf{r}}$*,* $\vec{\sigma}, \vec{\tau}$*, moving to a new position* $\tilde{\mathbf{r}}'$*, defined by direction cosines* $\alpha'_1, \alpha'_2, \alpha'_3$*.*